

## Highlights

### **Adapting Medical Vision Foundation Models for Volumetric Medical Image Segmentation via Active Learning and Selective Semi-supervised Fine-tuning**

Jin Yang, Daniel S. Marcus, Aristeidis Sotiras

- We are the first one to propose an Active Source-free Domain Adaptation method to adapt Medical Vision Foundation Models to target evaluation domains in volumetric medical image segmentation, achieving high adaptation performance and efficiency. This method employs a novel Active Test Time Sample Query strategy to query informative samples for fine-tuning, thus maximizing their performance. Additionally, it employs a novel Selective Semi-supervised Fine-tuning method to further optimize Medical Vision Foundation Models in a semi-supervised learning.
- The Active Test Time Sample Query strategy employs two novel query metrics, termed Diversified Knowledge Divergence (DKD) and Anatomical Segmentation Difficulty (ASD). DKD is designed to query samples with large source dissimilarity and intra-domain diversity by measuring their unlearned target knowledge and diversity. Additionally, ASD is proposed to query samples with large difficulty in segmentation of anatomical structure by evaluating the information levels in foreground regions adaptively.
- We propose a Selective Semi-supervised Fine-tuning method to fine-tune Medical Vision Foundation Models efficiently by leveraging reliable unannotated samples with their high quality pseudo labels and queried samples in a semi-supervised manner. The reliability of these samples are evaluated by the predictive confidence and their semantic distance to annotated samples.
- We implemented extensive experiments to evaluate the effectiveness of our ASFDA method on five volumetric medical image segmentation tasks. Our method outperformed other state-of-the-art AL and ADA methods.

# Adapting Medical Vision Foundation Models for Volumetric Medical Image Segmentation via Active Learning and Selective Semi-supervised Fine-tuning

Jin Yang<sup>a</sup>, Daniel S. Marcus<sup>a</sup> and Aristeidis Sotiras<sup>a,b,✉</sup>

<sup>a</sup>*Mallinckrodt Institute of Radiology, Washington University School of Medicine in St. Louis, St. Louis, 63110, MO, USA*

<sup>b</sup>*Institute for Informatics, Data Science and Biostatistics, Washington University School of Medicine in St. Louis, St. Louis, 63110, MO, USA*

---

## ARTICLE INFO

**Keywords:**

Vision Foundation Models  
Domain Adaptation  
Active Learning  
Semi-supervised Learning  
Medical Image Segmentation

---

## ABSTRACT

Medical Vision Foundation Models (Med-VFMs) have superior capabilities of interpreting medical images due to the knowledge learned from self-supervised pre-training with extensive unannotated images. To improve their performance on adaptive downstream evaluations, especially segmentation, a few samples from target domains are selected randomly for fine-tuning them. However, there lacks works to explore the way of adapting Med-VFMs to achieve the optimal performance on target domains efficiently. Additionally, random selection does not always capture informative samples from target domains, limiting the adaptation performance. Thus, it is highly demanded to design an efficient way of fine-tuning Med-VFMs by selecting informative samples to maximize their adaptation performance on target domains. To achieve this, we propose an Active Source-Free Domain Adaptation (ASFDA) method to efficiently adapt Med-VFMs to target domains for volumetric medical image segmentation. This ASFDA employs a novel Active Learning (AL) method to select the most informative samples from target domains for fine-tuning Med-VFMs without the access to source pre-training samples, thus maximizing their performance with the minimal selection budget. In this AL method, we design an Active Test Time Sample Query strategy to select samples from the target domains via two query metrics, including Diversified Knowledge Divergence (DKD) and Anatomical Segmentation Difficulty (ASD). DKD is designed to measure the source-target knowledge gap and intra-domain diversity. It utilizes the knowledge of pre-training to guide the querying of source-dissimilar and semantic-diverse samples from the target domains. ASD is designed to evaluate the difficulty in segmentation of anatomical structures by measuring predictive entropy from foreground regions adaptively. Thus, instead of considering the informativeness of the whole samples, it allows the querying of samples with high information levels in the region of interest. Additionally, our ASFDA method employs a Selective Semi-supervised Fine-tuning to improve the performance and efficiency of fine-tuning. It identifies samples with high reliability from unqueried ones if Med-VFMs are more likely to generate high-quality pseudo labels for them. These samples with their pseudo labels are combined with queried samples with their annotations to fine-tune Med-VFMs in a semi-supervised manner. To our knowledge, our work is the first one to adapt Med-VFMs to achieve the optimal performance on volumetric medical image segmentation efficiently via active learning and selective semi-supervised fine-tuning. We adapted Med-VFMs to five domains for volumetric medical image segmentation by our method to demonstrate its effectiveness. Our method achieved superior performance on these tasks than other state-of-the-art methods.

---

## 1. Introduction

Medical Visual Foundation Models (Med-VFMs) have superior capabilities of interpreting medical imaging and have demonstrated impressive ability in various medical image analysis tasks (Zhang and Metaxas, 2024). These Med-VFMs employ convolutional neural networks or Vision Transformers as basic architectures and are pre-trained on diversified unannotated imaging data via self-supervised learning (Moor et al., 2023; Zhou et al., 2023; Pai et al., 2025; Wang et al., 2025; Zhu et al., 2025). They are applied to non-adaptive downstream tasks for zero-shot predictions, demonstrating superior performance due to the intrinsic knowledge learned from pre-training. In contrast, when they are employed for downstream evaluation of adaptive tasks, including classification and segmentation, they demonstrate

low performance of zero-shot predictions on new domains. Specifically, when Med-VFMs are employed for segmenting target organs in unseen domains, they are incorporated with a newly initialized decoder with the symmetric architecture to generate an encoder-decoder segmentation network. Thus, this segmentation network has not been fine-tuned to capture target extrinsic features via fully supervised training, and they are not capable to accurately recognize extrinsic patterns of target organs.

To boost the performance of Med-VFMs on adaptive downstream evaluation, especially segmentation, some samples from target evaluation domains are selected for fine-tuning, equipping Med-VFMs with the capabilities of recognizing extrinsic target patterns. Random selection is usually implemented to achieve it (Pai et al., 2025). However, fine-tuning Med-VFMs by randomly selected samples cannot ensure to maximize the performance and efficiency of fine-tuning since informative samples cannot always be selected.

---

<sup>✉</sup>Corresponding author

 aristeidis.sotiras@wustl.edu (A. Sotiras)  
ORCID(s):

To address this limitation, active learning (AL) can be implemented to select the most informative samples from target domains for model optimization iteratively, thus maximizing the model performance with the minimal query budgets (Settles, 2011). These AL methods are employed to query informative samples by designing different query strategies to evaluate the predictive uncertainty and sample diversity (Siddiqui et al., 2020; Wu et al., 2021; Xie et al., 2022; Li et al., 2023a; Yang et al., 2024). When these AL methods are employed to adapt models across domains, these Active Domain Adaptation (ADA) methods utilize query strategies to select the most informative samples from target domains for optimizing them on these domains (Ning et al., 2021; Du and Li, 2023; Zhang et al., 2024).

However, applying these AL and ADA methods to actively adapt Med-VFMs to target domains in downstream tasks have three limitations. First, these methods lack mechanisms to query the most informative samples by leveraging the knowledge learned from pre-training. These methods are designed to adapt models without pre-training, mostly U-Net Ronneberger et al. (2015). However, evaluating the sample informativeness by leveraging the pre-training knowledge from Med-VFMs facilitates the quantification of unlearned knowledge in target domains, thus improving the adaptation performance and efficiency. Second, these methods employ query strategies to evaluate information levels on the whole images or volumes. However, measuring image-level informativeness of target samples may misestimate their information levels due to the imbalance between foreground and background regions. Organs of interest take a small foreground region in the whole image compared with background. Thus, evaluating sample-level information levels leads these methods to query samples with a high information level in the background while under-estimating the information level of foreground organs. Thus, these methods cannot query samples with informative foreground patterns for fine-tuning, limiting Med-VFMs from capturing organ-related target features. Third, source pre-training data or their annotations are unavailable, thus limiting the applicability of these methods. Specifically, strict data privacy regulations in clinical practice may limit query strategies from accessing source data. Additionally, Med-VFMs are pre-trained by unannotated samples via self-supervised learning, so their annotations are unavailable for these methods in the evaluation of informativeness. Although some Active Source-free Domain Adaptation (ASFDA) techniques are proposed to adapt models to target domains without access to the source data (Wang et al., 2023; Li et al., 2023b), their performance is challenged by the first two limitations.

Employing AL or ADA methods to query samples from target domains to optimize Med-VFMs may boost their performance by using queried samples for fine-tuning. However, this optimization is inefficient since models are fine-tuned using queried samples while unqueried samples are excluded due to the lack of annotations. To improve the performance of optimization, some semi-supervised learning methods are proposed and incorporated into ADA methods

(Wang et al., 2024a, 2022; He et al., 2024). These methods leverage the optimized networks to generate pseudo-labels for unlabeled samples, and subsequently, labeled samples and these unlabeled samples with their pseudo-labels are utilized to jointly optimize the networks. However, utilizing all unannotated samples with their pseudo labels for semi-supervised fine-tuning has two drawbacks to lower adaptation performance. First, networks have not fully captured extrinsic patterns from target domains in the first several AL iterations, so they will generate low-quality pseudo-labels for some unannotated samples. Thus, using them for fine-tuning may lead Med-VFMs to learn inaccurate patterns, thus lowering performance. Second, the relative ratio of queried samples to unannotated samples is small, so unannotated samples with their pseudo labels may be overwhelming over annotation samples, thus diverging the network to learn accurate patterns from queried samples and their annotations.

To tackle these limitations, we propose a novel **Active Source-free Domain Adaptation** method to adapt Medical Vision Foundation Models to target domains for volumetric medical image segmentation efficiently. This method employs a novel **Active Learning** method to query the most informative target samples for fine-tuning, thus maximizing the performance of Med-VFMs with the minimal queried samples. It also employs a **Selective Semi-supervised Fine-tuning** to select reliable unqueried samples for further optimizing Med-VFMs by them and queried samples in a semi-supervised learning. In AL method, we propose an **Active Test Time Sample Query** strategy to query the most informative target samples by employing two novel query metrics, termed **Diversified Knowledge Divergence** (DKD) and **Anatomical Segmentation Difficulty** (ASD). DKD is proposed to query samples with unlearned prior knowledge by evaluating semantic gaps between the source pre-training and target adapting domains. It also measures the semantic diversity among samples within the target domain during querying. Specifically, DKD calculates Prior and Adaptive Knowledge Divergence to measure knowledge gaps between source and target domains by identifying source-dissimilar samples. It also evaluates intra-domain diversity during querying by penalizing samples which demonstrate large intra-domain similarity. Additionally, ASD is proposed to evaluate difficulty in segmentation of anatomical structures by measuring information levels in foreground region of interest adaptively. Thus, querying samples by ASD to fine-tune Med-VFMs enables them to capture unlearned knowledge from samples with complex anatomical structures, thus achieving more accurate segmentation. Finally, informative samples are queried based on their DKD and ASD metric scores jointly.

After querying samples for annotations, we propose a Selective Semi-supervised Fine-tuning strategy to fine-tune Med-VFMs in a semi-supervised learning. This strategy allows the efficient fine-tuning by leveraging labeled and

a specific number of selected unlabeled samples, thus improving adaptation performance over fully-supervised fine-tuning. In this strategy, we implement a selective mechanism to select a specific ratio of unannotated samples with high reliability instead of utilizing all unannotated samples. Their reliability is evaluated based on their predictive confidence and semantic distance. Thus, samples with the highest confidence in their predictive probabilities and the smallest semantic distance to queried samples will be selected since the models are more likely to generate high-quality pseudo labels for them. Incorporating these samples with high-quality pseudo-labels alongside the actively selected samples in the semi-supervised fine-tuning facilitates further refinement of Med-VFMs, leading to improved performance and generalization.

To demonstrate the effectiveness of our Active Source-free Domain Adaptation method, we evaluated it by adapting Med-VFMs to five domains in volumetric medical image segmentation. These domains have large variations in imaging modalities, the number of structures to be segmented, and the number of samples. Our method demonstrates superior performance on these five datasets over other state-of-the-art AL and ADA methods. Our contributions can be summarized as follows:

- We are the first one to propose an Active Source-free Domain Adaptation method to adapt Medical Vision Foundation Models to target evaluation domains in volumetric medical image segmentation, achieving high adaptation performance and efficiency. This method employs a novel Active Test Time Sample Query strategy to query informative samples for fine-tuning, thus maximizing their performance. Additionally, it employs a novel Selective Semi-supervised Fine-tuning method to further optimize Medical Vision Foundation Models in a semi-supervised learning.
- The Active Test Time Sample Query strategy employs two novel query metrics, termed Diversified Knowledge Divergence (DKD) and Anatomical Segmentation Difficulty (ASD). DKD is designed to query samples with large source dissimilarity and intra-domain diversity by measuring their unlearned target knowledge and diversity. Additionally, ASD is proposed to query samples with large difficulty in segmentation of anatomical structure by evaluating the information levels in foreground regions adaptively.
- We propose a Selective Semi-supervised Fine-tuning method to fine-tune Medical Vision Foundation Models efficiently by leveraging reliable unannotated samples with their high quality pseudo labels and queried samples in a semi-supervised manner. The reliability of these samples are evaluated by the predictive confidence and their semantic distance to annotated samples.
- We implemented extensive experiments to evaluate the effectiveness of our ASFDA method on five

volumetric medical image segmentation tasks. Our method outperformed other state-of-the-art AL and ADA methods.

## 2. Related Works

### 2.1. Active Learning in Medical Image Segmentation

Active learning has been applied to achieve efficient medical image segmentation by identifying the most informative samples to optimize models with the minimal annotation cost. Suggestive Annotation is designed for the fully convolutional network to utilize uncertainty and similarity information to determine the most representative and uncertain samples for annotations (Yang et al., 2017). Bayesian U-Net utilizes Monte Carlo dropout in active learning to select samples with the large uncertainty for annotation to achieve muscle segmentation from clinical CTs (Hiasa et al., 2019). To explore the benefits of active learning for deep learning-based medical image segmentation, a query-by-committee framework is proposed to estimate uncertainty by multiple models (Nath et al., 2020). A deep active semi-supervised learning framework, DSAL, is proposed to select informative samples with high uncertainties and low uncertainties for strong labeling and weak labeling to efficiently utilize model knowledge for medical image segmentation (Zhao et al., 2021). A Hybrid Active Learning framework using Interactive Annotation is proposed to utilize a hybrid sample selection strategy to query samples for annotation by measuring pixel entropy, regional consistency and image diversity (Li et al., 2023c). Active learning with stochastic batches is proposed to query batches by evaluating batch-level uncertainty and employing sampling with randomness for efficient medical image segmentation (Gaillochet et al., 2023). SBC-AL employs an efficient query strategy to select samples with large uncertainty in the consistency of anatomical structure and boundary regions during active learning-based medical image segmentation (Zhou et al., 2024). An active learning method is proposed to query representative samples based on image similarity for skin lesion segmentation (Shu et al., 2025).

### 2.2. Active Source-Free Domain Adaptation in Medical Image Analysis

A few Active Source-Free Domain Adaptation methods have been proposed for medical image analysis, including segmentation and classification. A novel Guided Attention Transfer Network (GATN) and an active learning function are employed to adapt models from source domains to target domains (Kothandaraman et al., 2023). An Active Learning with Feature Disentanglement and Domain Adaptation is proposed to query representative samples based on domain specific and task specific image features for annotation in medical image classification (Mahapatra et al., 2024). A Source-domain and Target-domain Dual-Reference (STDR) strategy was proposed for the segmentation of nasopharyngeal carcinoma tumors from MR images across multiple

domains (Wang et al., 2024a). This strategy was designed to actively select representative domain-invariant and domain-specific samples for annotations by utilizing references to demonstrate the distributional characteristics of the source domain and the target domain. Additionally, an Uncertainty-guided method was proposed to adapt segmentation networks to different domains in prostate segmentation from MR images (Luo et al., 2024). This method is implemented to actively select samples with high uncertainty and diversity by employing a Global Aleatoric Uncertainty Aggregation to estimate slice-wise uncertainty and k-means to group diverse samples. ASFDA was utilized for vessel segmentation from Ultra-Wide-Field Scanning Laser Ophthalmoscopy (UWF-SLO) images (Wang et al., 2024b). In this adaptation task, after the whole UWF-SLO image was split into patches, patches with high foreground certainty were selected actively for annotations by implementing a Cascade Uncertainty-Predominance Selection strategy.

### 2.3. Medical Vision Foundation Models

Several foundation models have been proposed to interpret medical images with different modalities. Specifically, generalist medical AI was built by self-supervision on large medical data with diverse modalities to achieve superior capabilities of various downstream tasks (Moor et al., 2023). RETFound was developed as a foundation model for retinal images that learns generalizable representations from unlabeled retinal images and can be adapted to various applications efficiently (Zhou et al., 2023). CT-FM was developed as a large-scale 3D image-based CT foundation model pre-trained by label-agnostic contrastive learning using a large number of CT images (Pai et al., 2025). Triad was pre-trained as a vision foundation model on extensive MR images to learn general representations and interpret 3D MR imaging (Wang et al., 2025). FM-CT was pre-trained as a vision foundation model on head CT images using self-supervised learning for generalizable disease diagnosis (Zhu et al., 2025).

## 3. Methods

### 3.1. Overall Methods

The Medical Vision Foundation Model (Med-VFM) was pre-trained on extensive unannotated images  $\mathbf{X}_s$  of a specific modality  $\mathcal{M}_s$  with the number  $\mathcal{N}_s$  from source domain  $\mathbb{S} = \{\mathbf{X}_s\} = \{x_1, x_2, \dots, x_{\mathcal{N}_s} | \mathcal{M}_s\}$  via self-supervised learning. To evaluate the Med-VFM on downstream adaptive segmentation tasks, the pre-trained Med-VFM is employed as an encoder  $E$ , and incorporated with a symmetric decoder  $D$  into a U-shaped architecture, generating the segmentation model  $\mathcal{F}(\Theta; [E; D])$ . This segmentation model is evaluated on unlabeled data from a target domain via fine-tuning. This target domain includes images  $\mathbf{X}_t$  with the number  $\mathcal{N}_t$  of the modality  $\mathcal{M}_t$  as  $\mathbb{T} = \{\mathbf{X}_t\} = \{x_1, x_2, \dots, x_{\mathcal{N}_t} | \mathcal{M}_t\}$ .

As shown in Algorithm 1, the goal of the Active Source-Free Domain Adaptation (ASFDA) is to derive the Med-VFM-based segmentation model with source pre-trained

prior knowledge to boost evaluation performance on the target data  $\mathbf{X}_t$  without access to the source data  $\mathbf{X}_s$ . During downstream evaluation, the ASFDA method implements Active Learning (AL) to fine-tune the pre-trained Med-VFM-based segmentation network. This AL procedure is implemented to optimize the network iteratively for  $\mathcal{R}$  rounds, and it employs a novel Active Test Time Sample Query strategy to query a small number  $\mathcal{N}_B$  of informative samples from the target domain  $\mathbb{T}$  for annotations during test time at each round. Thus, the total number of queried samples is  $\mathcal{N}_{AL} = \mathcal{N}_B \cdot \mathcal{R}$  ( $\mathcal{N}_{AL} << \mathcal{N}_t$ ). These queried samples with their annotations are utilized to fine-tune the segmentation network, thus maximizing its evaluation performance on this domain with the minimal query budgets.

During initialization, the encoder is pre-trained on source data  $\mathbf{X}_s$  as  $E^{(p)}(\mathbf{X}_s)$  by capturing prior knowledge, and the decoder is newly initialized as  $D^{(0)}$  with a symmetric architecture. Thus, the network  $\mathcal{F}(\Theta)$  is constructed as  $\mathcal{F}(\Theta; [E^{(p)}(\mathbf{X}_s); D^{(0)}])$ . All images in this target domain  $\mathbb{T}$  are unannotated, so the unlabeled target set is initialized by  $\mathbb{T}_u = \mathbb{T}$ , and the labeled target set is empty as  $\mathbb{T}_l = \emptyset$ . At the beginning of the AL procedure before fine-tuning ( $r = 0$ ), the first target samples  $x_1$  with its annotation  $y_1$  is selected to optimize the network as  $\mathcal{F}^{(0)}(\Theta)$ . This sample is queried to the labeled target set as  $\mathbb{T}_l = \mathbb{T}_l \cup \{(x_1, y_1)\}$  and update the unlabeled target set as  $\mathbb{T}_u = \mathbb{T}_u \setminus \{x_1\}$ .

Subsequently, the AL procedure is implemented as follows. At the first round  $r = 1$ , we implement the Active Test Time Sample Query strategy to actively query  $\mathcal{N}_B$  instances from the unlabeled target set  $\mathbb{T}_u$  for annotation based on their DKD and ASD metric scores. These samples  $\mathbf{X}_t^1 = \{x_1, \dots, x_{\mathcal{N}_B}\}$  with their annotations  $\mathbf{Y}_t^1 = \{y_1, \dots, y_{\mathcal{N}_B}\}$  are queried to the labeled target set  $\mathbb{T}_l = \mathbb{T}_l \cup \{(\mathbf{X}_t^1, \mathbf{Y}_t^1)\}$ , and the unlabeled target set is updated as  $\mathbb{T}_u = \mathbb{T}_u \setminus \{\mathbf{X}_t^1\}$ . Subsequently, this labeled target set is utilized to optimize the model as  $\mathcal{F}^{(1)}(\Theta)$  via Selective Semi-supervised Fine-tuning. This fine-tuning is implemented to optimize the network in three stages. Specifically, the network is optimized as  $\mathcal{F}^{(1)}(\Theta)$  by the images  $\mathbf{X}_{t,l}^1$  with their annotations  $\mathbf{Y}_{t,l}^1$  from the labeled target set  $\mathbb{T}_l$  in a fully-supervised manner. Then a specific number  $\mathcal{N}_{SU}$  of unlabeled samples  $\mathbf{X}_{t,u}^1 = \{x_1, x_2, \dots, x_{\mathcal{N}_{AL}}\}$  are selected from the unlabeled target set  $\mathbb{T}_u$  based on predictive confidence and semantic distance, and the number of selected unlabeled samples is equal to the number of labeled samples  $\mathcal{N}_{SU} = \mathcal{N}_B \cdot r$ . The network is employed to generate their pseudo labels  $\mathbf{Y}_{t,u}^1 = \{y_1, y_2, \dots, y_{\mathcal{N}_{AL}}\}$ . In the third stage, these selected samples  $\mathbf{X}_{t,u}^1$  and their pseudo-labels  $\mathbf{Y}_{t,u}^1$  are combined with samples from the labeled target set  $\mathbb{T}_l$  as a new set  $\mathbb{T}_{l,p} = \mathbb{T}_l \cup \{(\mathbf{X}_{t,u}^1, \mathbf{Y}_{t,u}^1); \mathcal{M}_t\}$  to fine-tune the network  $\mathcal{F}^{(1)}(\Theta)$  in a semi-supervised manner. The AL is implemented in  $\mathbb{T}_u$  for the next round. In subsequent each round ( $r > 1$ ),  $\mathcal{N}_B$  samples  $\mathbf{X}_t^r = \{x_1, \dots, x_{\mathcal{N}_B}\}$  are queried for their annotations  $\mathbf{Y}_t^r = \{y_1, \dots, y_{\mathcal{N}_B}\}$  by the Active Test Time Sample Query strategy, generating the updated labeled target set  $\mathbb{T}_l = \mathbb{T}_l \cup \{(\mathbf{X}_t^r, \mathbf{Y}_t^r); \mathcal{M}_t\}$  and unlabeled target set  $\mathbb{T}_u =$

**Algorithm 1** Active Source-Free Domain Adaptation of Medical Vision Foundation models

**Input:** Pre-trained Encoder  $E^{(p)}(\mathbf{X}_s)$ ; Initialized decoder  $D^{(0)}$ ; Samples from unlabeled target domain  $\mathbb{T} = \{\mathbf{X}_t\} = \{x_1, \dots, x_t, \dots, x_{N_t}\}$ ; Maximum AL round  $\mathcal{R}$ ; Query budget  $\mathcal{N}_B$ ; Total query budget  $\mathcal{N}_{AL}$ ; Selected unlabeled budget  $\mathcal{N}_{SU}$ .

**Output:** target-optimized Med-VFM-based segmentation network  $\mathcal{F}(\Theta^*)$ .

**Begin:**

- 1: Let current round  $r = 0$ ;
- 2: Construct  $\mathcal{F}(\Theta) \leftarrow \mathcal{F}^{(0)}(\Theta; [E^{(p)}; D^{(0)}])$  as the segmentation network;
- 3: Initialize  $\mathbb{T}_l \leftarrow \emptyset$ ,  $\mathbb{T}_u \leftarrow \mathbb{T}$ ;
- 4: **while**  $r \leq \mathcal{R}$  **do**
- 5:   **if**  $r == 0$  **then**
- 6:     Select  $x_1$  with its label  $y_1$  from  $\mathbb{T}$  to optimize  $\mathcal{F}(\Theta)$  as  $\mathcal{F}^{(0)}(\Theta)$ ;
- 7:     Update  $\mathbb{T}_l \leftarrow \mathbb{T}_l \cup \{(x_1, y_1)\}$ ,  $\mathbb{T}_u \leftarrow \mathbb{T}_u \setminus \{x_1\}$ ;
- 8:     Continue;
- 9:   **end if**
- 10:   Calculate DKD( $x_u$ ) on samples  $x_u$  from  $\mathbb{T}_u$  by Eq.5;
- 11:   Calculate ASD( $x_u$ ) on samples  $x_u$  from  $\mathbb{T}_u$  by Eq.11;
- 12:   Calculate  $Q(x_u)$  by Eq.16;
- 13:   Query  $\mathcal{N}_B$  samples  $\mathbf{X}_t^r$  with the largest scores for annotations  $\mathbf{Y}_t^r$  by Oracle;
- 14:   Update  $\mathbb{T}_l \leftarrow \mathbb{T}_l \cup \{(\mathbf{X}_t^r, \mathbf{Y}_t^r)\}$ ,  $\mathbb{T}_u \leftarrow \mathbb{T}_u \setminus \{\mathbf{X}_t^r\}$ ;
- 15:   Fine-tune the network as  $\mathcal{F}^{(r)}(\Theta)$  by images  $\mathbf{X}_l$  with their annotations  $\mathbf{Y}_l$  from  $\mathbb{T}_l$ ;
- 16:   Select  $\mathcal{N}_{SU}$  unlabeled samples  $\mathbf{X}_{t,u}^r$  from  $\mathbb{T}_u$  by Eq.26;
- 17:   Generate pseudo labels  $\mathbf{Y}_{t,u}^r$  for  $\mathbf{X}_{t,u}^r$  by  $\mathcal{F}^{(r)}(\Theta)$ ;
- 18:   Update  $\mathbb{T}_{l,p} \leftarrow \mathbb{T}_l \cup \{(\mathbf{X}_{t,u}^r, \mathbf{Y}_{t,u}^r)\}$ ;
- 19:   Fine-tune the network  $\mathcal{F}^{(r)}(\Theta)$  by  $\mathbb{T}_{l,p}$  in a semi-supervised learning;
- 20:    $r \leftarrow r + 1$ ;
- 21: **end while**

**End**

$\mathbb{T}_u \setminus \{\mathbf{X}_t^r\}$ . This updated labeled target set  $\mathbb{T}_l$  is utilized to continuously optimize the network as  $\mathcal{F}^{(r)}(\Theta)$ . Then  $\mathcal{N}_{SU}$  unlabeled samples  $\mathbf{X}_{t,u}^r$  are selected for generating pseudo-labels  $\mathbf{Y}_{t,u}^r$ . The Selective Semi-supervised Fine-tuning is implemented to fine-tune the network by the set  $\mathbb{T}_{l,p} = \mathbb{T}_l \cup \{(\mathbf{X}_{t,u}^r, \mathbf{Y}_{t,u}^r)\}$  in a semi-supervised manner. The iterations will be terminated until the labeled target samples reach the pre-defined annotation budgets  $\mathcal{N}_{AL}$  or the AL procedure is implemented to the maximal rounds  $\mathcal{R}$ . The whole AL procedure is implemented to optimize the network to achieve the optimal performance as  $\mathcal{F}(\Theta^*)$  with the minimal query budgets on the target domain  $\mathbb{T}$ .

### 3.2. Active Test Time Sample Query

Our ASFDA method employs an Active Test Time Sample Query strategy to select the most informative samples from target domains for annotation. This strategy utilizes

two query metrics to assess the informativeness of target samples, termed Diversified Knowledge Divergence (DKD) and Anatomical Segmentation Difficulty (ASD).

#### 3.2.1. Diversified Knowledge Divergence

To query samples with unlearned knowledge and intra-domain diversity, we propose a sample-level query metric, termed Diversified Knowledge Divergence (DKD). First, it calculates Prior and Adaptive Knowledge Divergence to evaluate the domainness by measuring the knowledge gap between source and target domains, and this gap is measured by identifying source-dissimilar samples from the target adapting domain. Thus, querying these target-specific samples for fine-tuning enables the network to capture domain-specific information, facilitating it to fit the target domains by learning new adaptive knowledge. Additionally, lacking the measurement of intra-domain diversity may lead to the query of samples with large similarity in the target domain. Thus, utilizing these samples for fine-tuning may lead the network to learn similar knowledge and capture overlapped information from the target domain, diminishing the efficiency of active fine-tuning. To tackle this limitation, intra-domain diversity is evaluated by calculating the Pair-wise Dissimilarity for target samples.

First, the knowledge gap between the source pre-training domain and the target adapting domain is measured by calculating Prior and Adaptive Knowledge Divergence (PAKD). It is achieved by measuring the semantic dissimilarity between feature embeddings with prior and adaptive knowledge. Specifically, for an unlabeled image scan  $x_u \in \mathbb{R}^{H \times W \times D}$  from the unlabeled target set  $\mathbb{T}_u$  ( $H$ ,  $W$ , and  $D$  represent the height, width, and depth of a volume scan, respectively), the pre-trained encoder  $E^{(0)}$  before adaptation is employed to extract its prior knowledge by generating feature embeddings  $E^{(0)}(x_u)$ . Subsequently, the fine-tuned encoder  $E^{(i)}$  is employed to evaluate its adaptive knowledge by generating feature embeddings  $E^{(i)}(x_u)$ . The PAKD is calculated by measuring the cosine distance (CosDis) between these feature embeddings. The larger PAKD value demonstrates the larger dissimilarity. Thus, PAKD for the sample  $x_u$  is calculated as follows

$$\text{PAKD}(x_u) = \text{CosDis}(E^{(0)}(x_u), E^{(i)}(x_u)) \quad (1)$$

$$= 1 - \frac{E^{(0)}(x_u) \cdot E^{(i)}(x_u)^T}{\|E^{(0)}(x_u)\| \cdot \|E^{(i)}(x_u)\|} \quad (2)$$

Second, we propose to measure intra-domain diversity by calculating Pair-wise Dissimilarity (PD) rather than employing cluster-based diversity sampling methods. Utilizing cluster-based diversity sampling methods may lead the models to query outliers or domain-similar samples. Querying outliers to fine-tune Med-VFMs may distract them to learn the accurate intensity distribution of target domains. Additionally, clustering methods usually have a high computational complexity when they need to load feature embeddings for all samples into the memory for computation. To avoid these limitations, our PD is designed as a weighting term to penalizing samples which demonstrate

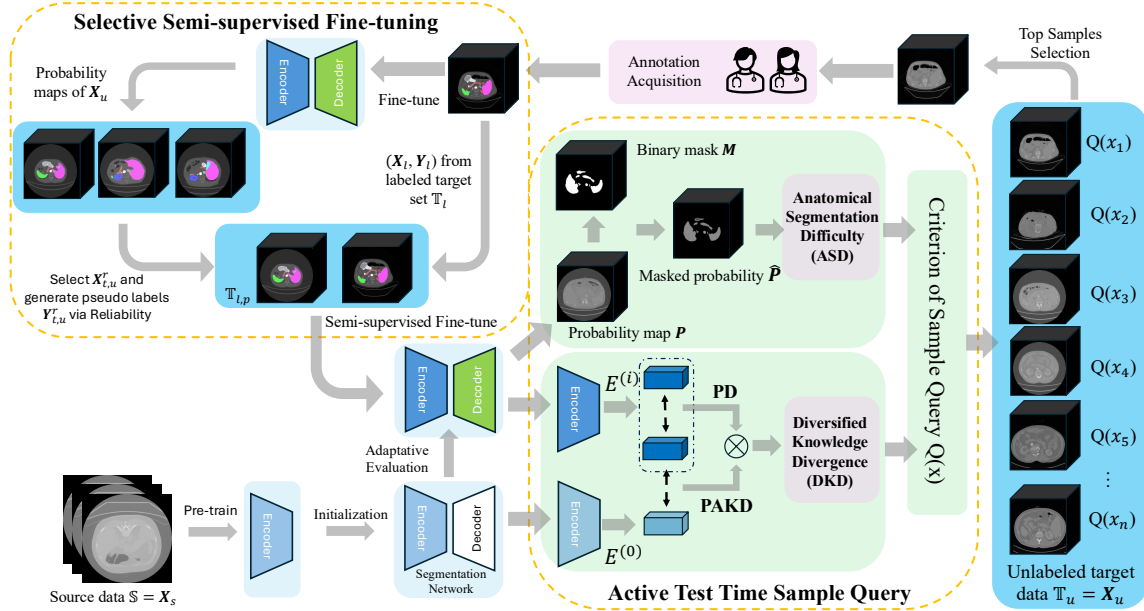


**Figure 1: Active Source-Free Domain Adaptation (ASFDA) of Medical Vision Foundation Models for volumetric medical image segmentation.** The segmentation network was pre-trained on the source data  $\mathbb{S} = \{X_s\}$  and adapted to the target domain  $\mathbb{T}$  for downstream evaluation. ASFDA employs an **Active Test Time Sample Query** strategy to evaluate the information level of each target sample. This strategy employs two metrics, including **Diversified Knowledge Divergence (DKD)** and **Anatomical Segmentation Difficulty (ASD)**. Subsequently, the scores of these two metrics are fused as criterion of sample query  $Q(x)$  for unlabeled target data  $\mathbb{T}_u = \{X_u\}$ . Top samples  $X_l$  with large query scores are collected for their annotations  $Y_l$ . These queried samples and their annotations are selected to fine-tune the network via a **Selective Semi-supervised Fine-tuning**. After fine-tuned by labeled data  $(X_l, Y_l)$ , the network makes predictions to generate probability maps for unlabeled target data  $X_u$ . Unlabeled data  $X_{t,u}^r$  are selected based on Reliability and their pseudo labels  $Y_{t,u}^r$  are generated. These data  $(X_{t,u}^r, Y_{t,u}^r)$  are combined with labeled data  $(X_l, Y_l)$  to fine-tune the network in a semi-supervised manner.

the large semantic similarity to samples with large PAKD scores. Specifically, all samples from the unlabeled target set  $\mathbb{T}_u = \{X_u\}$  are sorted in a descending order based on the scores of PAKD as  $x_u^1, x_u^2, \dots, x_u^c, \dots, x_u^{\mathcal{N}_u}$ . Subsequently, the PD term of the sample  $x_u^c$  is measured by calculating cosine distance between the feature embeddings of this sample  $x_u^c$  and the feature embeddings of all samples with larger PAKD values  $x_u^1, x_u^2, \dots, x_u^{c-1}$ . To enhance the importance of PAKD, the cosine distance between any two samples is weighted by the distance of their indices in this sorted array. The weighted cosine distance among the current sample and all other samples are summed and normalized by the total distance to ensure the PD has the same range as PAKD. The PD is designed as follows

$$PD(x_u^c) = \frac{\sum_{k=1}^{c-1} k * \text{ConDis}(E^{(i)}(x_u^c), E^{(i)}(x_u^{c-k}))}{\sum_{k=1}^{c-1} k} \quad (3)$$

$$= \frac{\sum_{k=1}^{c-1} k * (1 - \frac{E^{(i)}(x_u^c) \cdot E^{(i)}(x_u^{c-k})^T}{\|E^{(i)}(x_u^c)\| \cdot \|E^{(i)}(x_u^{c-k})\|})}{\sum_{k=1}^{c-1} k} \quad (4)$$

Finally, the DKD for the sample  $x_u$  is calculated by multiplying the PAKD value with its PD value as

$$DKD(x_u) = \text{PAKD}(x_u) \times PD(x_u) \quad (5)$$

### 3.2.2. Anatomical Segmentation Difficulty

Samples with complex patterns in anatomical structures may have a high segmentation difficulty level, leading the model to demonstrate large epistemic uncertainty in their predictions due to lack of knowledge. To measure the complexity of anatomical structures and unlearned knowledge of these target structures, we propose an organ-level query metric, termed Anatomical Segmentation Difficulty (ASD), to assess the difficulty level in sample segmentation by calculating entropy in the predictions. Instead of evaluating segmentation difficulty level in the whole sample, ASD is designed to evaluate it in the foreground region of interest adaptively to avoid the noise from background regions. Additionally, the foreground is extracted adaptively based on the network learning status and AL stage.

Specifically, for an image sample  $x_u \in \mathbb{R}^{H \times W \times D}$  from the target unlabeled set  $\mathbb{T}_u$ , the network  $\mathcal{F}(\Theta)$  generates predictive probability maps for  $C$  target classes as  $\mathbf{P} \in \mathbb{R}^{C \times H \times W \times D}$ , where  $C$  represents the number of channels and is equal to the number of segmentation classes. Specifically, the network generates  $C$  probability map  $\mathbf{P}_i \in \mathbb{R}^{H \times W \times D}$  to predict the probabilities of voxels in the sample  $x_u$  to the class, denoting  $\mathbf{P} = \{\mathbf{P}_0, \dots, \mathbf{P}_i, \dots, \mathbf{P}_{C-1}\} | i \in \{0, \dots, C-1\}\}$ . The segmentation classes include background and the target anatomical structures, so the first

probability map  $\mathbf{P}_0$  is the predictive probabilities of voxels to be classified to background.

First, the mis-segmentation tolerance is implemented to adjust the probabilities of background by applying a dynamic temperature scaling function to the predicted probability map of background  $\mathbf{P}_0$  based on the learning status and AL stage as

$$\mathbf{P}'_0 = \frac{\mathbf{P}_0}{\tau(r)} \quad (6)$$

where  $\tau(r)$  is a dynamic temperature scaling function. The value of the dynamic temperature scaling function decreases from 3 in the first round  $r = 1$  to 1.5 in the maximal round  $r = \mathcal{R}$  as

$$\tau(r) = -\frac{3}{2 \log \mathcal{R}} \log r + 3. \quad (7)$$

Subsequently, a binary mask  $\mathbf{M} \in \mathbb{R}^{H \times W \times D}$  is generated to segment foreground regions from background based on the tolerance-adjusted background probability map  $\mathbf{P}'_0$  and original probability maps for target organs  $\{\mathbf{P}_1, \dots, \mathbf{P}_{C-1}\}$

$$\mathbf{P}_{max} = \max([\mathbf{P}_1, \dots, \mathbf{P}_{C-1}]), \quad (8)$$

$$\mathbf{M} = \mathbb{1}[\mathbf{P}'_0 < \mathbf{P}_{max}]. \quad (9)$$

This mis-segmentation tolerance is utilized to reduce confidence in the prediction of background regions, thus avoiding false negatives when generating the binary mask. Instead of employing a fixed temperature scaling mechanism, we propose a dynamic temperature scaling function. The value of this function is determined by the learning status and AL stage dynamically, and decreases with the number of AL iteration  $r$ . Specifically, at the first several rounds, the segmentation is underperformed, so a larger temperature value is employed to avoid mis-segmented regions when generating binary masks. In contrast, the segmentation performance is improved significantly with AL optimization, a smaller temperature value is utilized to generate accurate masks.

Subsequently, the binary mask is applied to these probability maps  $\mathbf{P}$  to highlight foreground regions and avoid the influence of noise from background regions, generating foreground masked predictive probability maps  $\hat{\mathbf{P}} \in \mathbb{R}^{C \times H \times W \times D}$  as

$$\hat{\mathbf{P}} = \mathbf{P} \odot \mathbf{M}. \quad (10)$$

Lastly, the ASD score for the sample  $x_u$  is calculated to evaluate its information level by calculating the entropy from the foreground regions of the predictive probabilities as

$$ASD(x_u) = - \sum_{i=0}^{C-1} \hat{\mathbf{P}}_i(x_u) \log \hat{\mathbf{P}}_i(x_u). \quad (11)$$

### 3.2.3. Criterion of Sample Query

We normalize the DKD and ASD scores for unlabeled image  $x_u$  from the unlabeled target set  $\mathbb{T}_u$  via min-max

normalization to ensure these two scores are in the same range

$$\hat{DKD}(x_u) = \frac{DKD(x_u) - \min(DKD(x_u))}{\max(DKD(x_u)) - \min(DKD(x_u))}, \quad (12)$$

$$\hat{ASD}(x_u) = \frac{ASD(x_u) - \min(ASD(x_u))}{\max(ASD(x_u)) - \min(ASD(x_u))}. \quad (13)$$

To ensure DKD and ASD scores distributed uniformly in the range  $[0, 1]$  and avoid the overwhelming of one score over another one, we apply a uniform Quantile transformation technique to them as

$$\widehat{DKD}(x_u) = \text{QuanTrans}(\hat{DKD}(x_u)), \quad (14)$$

$$\widehat{ASD}(x_u) = \text{QuanTrans}(\hat{ASD}(x_u)). \quad (15)$$

We integrate quantile-transformed and unit-normalized DKD and ASD scores into a unified Active Test Time Sample Query selection criterion  $Q \in [0, 2]$  for the sample  $x_u$  from the unlabeled target set  $\mathbb{T}_u$  as

$$Q(x_u) = \widehat{DKD}(x_u) + \widehat{ASD}(x_u). \quad (16)$$

### 3.3. Selective Semi-supervised Fine-tuning

In the Selective Semi-supervised Fine-tuning, we employ a three-stage approach. In the first stage of the iteration  $r$ , we fine-tune the Med-VFM-based network  $\mathcal{F}^{(r)}(\Theta)$  by utilizing actively queried samples with their annotations  $\mathbb{T}_l = \{(\mathbf{X}_l, \mathbf{Y}_l); \mathcal{M}_l\}$  in a fully-supervised manner. This fine-tuning by actively queried samples enables the networks  $\mathcal{F}^{(r)}(\Theta)$  to capture more target-specific information and thus generate high-quality pseudo labels.

In the second stage, we select unlabeled samples  $\mathbf{X}_{t,u}^r$  from unlabeled target set  $\mathbb{T}_u$  and employ the network  $\mathcal{F}^{(r)}(\Theta)$  to generate pseudo labels  $\mathbf{Y}_{t,u}^r$  for semi-supervised learning based on two metrics, including semantic distance and predictive confidence. These unlabeled samples are selected if they demonstrate small semantic distance to labeled samples and fine-tuned Med-VFMs demonstrate high confidence in their probabilistic predictions. Specifically, if one unlabeled sample demonstrates a small semantic distance to labeled samples, it is highly likely that Med-VFMs have learned its semantic patterns by the fine-tuning in the first stage, and they can generate a high-quality predictive result. Additionally, if the network demonstrates large confidence in the probabilistic prediction of an unlabeled sample, it is likely to make an accurate prediction, thus generating a high-quality pseudo label.

To achieve this, first, we propose to calculate model confidence in predictions for all unlabeled samples  $\mathbf{X}_u = \{x_1, x_2, \dots, x_u\}$  from the unlabeled target set  $\mathbb{T}_u$  via foreground prediction margin. Specifically, a binary predicted mask  $\mathbf{M}_c \in \mathbb{R}^{H \times W \times D}$  is generated from predicted probability maps  $\mathbf{P}_c \in \mathbb{R}^{C \times H \times W \times D}$  of an unlabeled sample  $x_u$ . This binary mask is generated by assigning foreground and background labels to all foreground and background voxels, respectively as

$$\mathbf{M}_c(x_u) = \mathbb{1}[\arg \max_{c \in \{0, 1, \dots, C-1\}} \mathbf{P}_c(x_u) \neq 0]. \quad (17)$$

Subsequently, a largest probability map  $\mathbf{P}_{max}$  and a second largest one  $\mathbf{P}_{max}^{(2)}$  are generated from predicted probabilities  $\mathbf{P}_c \in \mathbb{R}^{C \times H \times W \times D}$  by extracting the largest and the second largest probabilities for each voxels as

$$\mathbf{P}_{max}(x_u) = \max \mathbf{P}_c(x_u), \quad (18)$$

$$\hat{\mathbf{P}}_{max}(x_u) = \max_{\mathbf{P}_c < \mathbf{P}_{max}} \mathbf{P}_c(x_u). \quad (19)$$

The network demonstrates high confidence in the background voxels, and foreground voxels occupy a small partition of voxels from the whole image volume. Thus, the predictive confidence in background voxels will overwhelm that in foreground voxels, and involving all voxels into the calculation of voxel-wise margin may over-estimate the sample confidence. To avoid this over-estimation of samples confidence, we apply the binary mask  $\mathbf{M}_c$  to highlight the probability of foreground voxels while suppressing the background voxels as

$$\hat{\mathbf{P}}_{max}(x_u) = \mathbf{P}_{max}(x_u) \odot \mathbf{M}_c(x_u), \quad (20)$$

$$\hat{\mathbf{P}}_{max}^{(2)}(x_u) = \mathbf{P}_{max}^{(2)}(x_u) \odot \mathbf{M}_c(x_u). \quad (21)$$

The confidence  $C(x_u)$  of this sample  $x_u$  is evaluated by calculating voxel-wise margin between the binary-masked largest and the binary-masked second largest probabilities and summarized of all voxels  $v$  across the whole volume  $V$  as

$$C(x_u) = \sum_{v \in V} (\hat{\mathbf{P}}_{max}(x_u) - \hat{\mathbf{P}}_{max}^{(2)}(x_u)). \quad (22)$$

If models demonstrate low predictive confidence on samples, they are unlikely to generate accurate predictions on these samples. To reduce the selection burdens in the following steps, we pre-select top  $\mathcal{K}$  samples with high confidence as the candidates  $\mathbf{X}_k$  for the next step while filtering out others based on learning status of the models. The learning status of the models is estimated by averaging the confidence over all unlabeled samples  $\mathbf{X}_u$  from the unlabeled target set  $\mathbb{T}_u$  as

$$\bar{C} = \frac{\sum_{x_u \in \mathbf{X}_u} C(x_u)}{U} \quad (23)$$

where  $U$  is the number of samples from the the unlabeled target set  $\mathbb{T}_u$ . Thus, the number of selected candidates is determined by

$$\mathcal{K} = \frac{\mathcal{N}_{SU}}{\bar{C}/\tau_c}. \quad (24)$$

$\tau_c$  is the temperature to reduce the predictive confidence. Subsequently, we create anchors by employing the encoder  $E^{(r)}$  of fine-tuned Med-VFMs to generate feature embeddings for queried samples  $x_l$  in the labeled set  $\mathbb{T}_l$  as  $\mathbf{A}^{(r)} = E^{(r)}(x_l)$ . This encoder  $E^{(r)}$  is also employed to generate feature embeddings from those high confidence candidates  $\mathbf{X}_k = \{x_1, \dots, x_k, \dots, x_{\mathcal{K}}\}$  as  $\mathbf{F}^{(r)}(x_k) = E^{(r)}(x_k)$ . The

semantic distance  $D(x_k)$  of a sample  $x_k$  is measured by calculating the minimal cosine distance between its embeddings and all anchors as

$$D(x_k) = \min_{a \in \mathbf{A}^{(r)}} [\text{CosDis}(\mathbf{A}^{(r)}, \mathbf{F}^{(r)}(x_k))]. \quad (25)$$

We calculate reliability  $R$  for these candidates  $\mathbf{X}_k$  based on their predictive confidence  $C$  and their sematic distance  $D$  as

$$R(x_k) = C(x_k) \times (1 - D(x_k)). \quad (26)$$

Unlabeled samples are selected from  $\mathcal{K}$  candidates  $\mathbf{X}_k$  for Med-VFMs to generate pseudo labels. To achieve a balance in semi-supervised fine-tuning, the number of selected unlabeled samples is equal to the number of labeled samples  $\mathcal{N}_{SU} = \mathcal{N}_B \cdot r$ . In the last stage, we employ Med-VFMs to generate high-quality pseudo labels  $\mathbf{Y}_{t,u} = \{y_1, y_2, \dots, y_{t,u}\}$  for these selected unlabeled samples  $\mathbf{X}_{t,u} = \{x_1, x_2, \dots, x_{t,u}\}$  with the largest reliability value. These selected samples and their pseudo labels are combined with queried samples as a new set  $\mathbb{T}_{l,p} = \mathbb{T}_l \cup \{(\mathbf{X}_{t,u}^r, \mathbf{Y}_{t,u}^r); \mathcal{M}_t\}$  to fine-tune the Med-VFMs in a semi-supervised manner.

### 3.4. Uninformative Samples Exclusion

In the selective semi-supervised fine-tuning,  $\mathcal{N}_{SU}$  unlabeled samples  $\mathbf{X}_{t,u}$  are selected. These samples show small semantic distance to labeled samples, and Med-VFMs demonstrate large confidence in their predictions. Thus, these samples demonstrate large overlapping in the information with labeled samples, and querying them is not able to provide high informativeness to Med-VFMs. To reduce the burdens of active querying, we exclude these selected samples from the process of active sample querying in the next AL round.

### 3.5. The Architecture of Med-VFM-based Segmentation Network

The segmentation network is built as an U-shape encoder-decoder architecture based on CT-FM (Pai et al., 2025). This network has five layers, including a bottleneck and the number of feature maps in each layer was 32, 64, 256, 512, and 1024, respectively. The residual segmentation block is employed to extract features at each layer in the encoder and the decoder, and the number of residual block was 1, 2, 2, 4, and 4 in these layers. Each residual block consists of two cascading convolutional layers following a batch normalization layers and a ReLU function. The  $3 \times 3 \times 3$  convolutional layer with the stride of 2 is utilized for downsampling to downscale feature maps in the encoder, and the  $3 \times 3 \times 3$  transposed convolutional layer is used to upscale the feature maps for upsampling in the decoder. The skip-connected features from the encoder are fused with those upsampled in the decoder at the same layer via channel-wise addition. At the initial layer, a  $3 \times 3 \times 3$  convolutional layer is employed to convert the number of feature maps from the number of input channels to 32. At the final layer, a  $1 \times 1 \times 1$  convolution is used to generate the segmentation prediction. The encoder

was pre-trained on extensive CT scans without ground truth annotations via self-supervised learning as demonstrated in CT-FM (Pai et al., 2025), and the decoder was initialized by Kaiming initialization on our own (He et al., 2015).

## 4. Experiments

### 4.1. Datasets

To evaluate the effectiveness of our methods, we adapt the Med-VFM-based segmentation network to five abdominal multi-organ segmentation datasets with large differences in the number of subjects, imaging modalities, and the number of organs to be segmented.

**AMOS2022-CT.** The AMOS2022-CT dataset is from the MICCAI 2022 AMOS abdominal multi-organ segmentation challenge (Ji et al., 2022). It consists of 300 abdominal CT volume scans with voxel-level annotations of 15 organ categories, including spleen, right kidney, left kidney, gallbladder, esophagus, liver, stomach, aorta, inferior vena cava, pancreas, right adrenal gland, left adrenal gland, duodenum, bladder, and prostate/uterus. Each CT volume consists of  $67 \sim 369$  slices of  $512 \times 512$  pixels with a slice spacing of  $1.25 \sim 5.00$  mm.

**FLARE 2021.** This dataset is from The Fast and Low GPU memory Abdominal ORgan sEgmentation (FLARE) challenge (Ma et al., 2022). It consists of 361 CT images with voxel-wise annotations of four abdominal organs, including the liver, the kidneys, the spleen, and the pancreas. It demonstrates a large diversity across various centers, vendors, phases, and diseases.

**Abdomen Atlas.** This dataset includes 9262 3D CT volumes with pre-voxel annotations of 25 anatomical structures, including 16 abdominal organs, two thorax organs, five vascular structures, and two skeletal structures (Li et al., 2025). These CT volumes are collected from 112 hospitals in 19 countries, generating this multi-center dataset.

**AMOS2022-MRI.** This dataset is from MICCAI 2022 AMOS abdominal multi-organ segmentation challenge (Ji et al., 2022). It consists of 60 abdominal MR volume scans with voxel-level annotations of 13 organ categories, including spleen, right kidney, left kidney, gallbladder, esophagus, liver, stomach, aorta, inferior vena cava, pancreas, right adrenal gland, left adrenal gland, and duodenum. Since only two cases have annotations of bladder and prostate/uterus, we removed these two labels from this dataset to avoid extreme class imbalance.

**Abdominal MRI.** This dataset is from the external evaluation of MRAnnotator (Zhou et al., 2025). We select 30 abdominal MR images from external evaluation with voxel-wise annotations of eight anatomical structures, including spleen, right kidney, left kidney, gallbladder, liver, aorta, inferior vena cava, and pancreas.

We applied the pre-processing strategy to imaging scans from these datasets. Specifically, the image intensities were clipped at the 5th and 95th percentiles, and then z-score normalization was applied to each volume. Subsequently, scans were cropped to sub-volumes as input patches with

a specific size. The patch size was  $96 \times 160 \times 160$  in the AMOS2022-CT dataset,  $96 \times 192 \times 160$  in the FLARE 2021 dataset,  $96 \times 128 \times 160$  in the Abdomen Atlas dataset,  $48 \times 160 \times 224$  in the AMOS2022-MRI dataset, and  $64 \times 192 \times 192$  in the Abdominal MRI dataset.

### 4.2. Implementation Details

The experiments were implemented using PyTorch<sup>1</sup>. A combination of dice loss  $\mathcal{L}_{Dice}$  and cross-entropy loss  $\mathcal{L}_{CE}$  was used as the loss function. The loss function  $\mathcal{L}$  can be formulated between the prediction  $\hat{y}$  and the ground truth  $y$  as follows

$$\mathcal{L} = \mathcal{L}_{Dice}(\hat{y}, y) + \mathcal{L}_{CE}(\hat{y}, y).$$

Models were trained with a batch size of 2 on NVIDIA Tesla A100 PCI-E Passive Single GPU with 40GB of GDDR5 memory. The AdamW was used as the optimizer. The network was trained for 100 epochs in one-shot initialization. Subsequently, the network was fine-tuned for 800 epochs at each round in the Abdomen Atlas domain, and 400 epochs at each round in other four domains. The learning rate was set to 0.0001 initially, and it decayed with a polynomial learning rate scheduler. During training, data augmentation techniques were implemented to improve model robustness. To be specific, patches were rotated between  $[-30, 30]$  along three axes with a probability of 0.2 and then scaled between (0.7, 1.4) with a probability of 0.2. Subsequently, all patches were mirrored along all axes with a probability of 0.5. Zero-centered additive Gaussian noise, with variance drawn from the distribution  $U(0, 0.1)$ , and brightness adjustments were added to each voxel sample with a probability of 0.15 for each. The segmentation performance was evaluated using the Dice coefficient score (Dice).

### 4.3. Active Learning Protocols.

We implemented different active learning protocols for these target sets since they have different segmentation complexity and imaging modalities. In AMOS2022-CT, FLARE 2021, and AMOS2022-MRI datasets, we implemented active domain adaptation to query samples to optimize the segmentation network on target domains iteratively. Specifically, the AL procedure in AMOS2022-CT and FLARE 2021 was implemented for five rounds ( $\mathcal{R} = 5$ ), and the query budget was 5% at each round ( $\mathcal{N}_B = 5\%$ ). In AMOS2022-MRI, we queried 5% ( $\mathcal{N}_B = 5\%$ ) samples at each round, and implemented AL querying for six rounds ( $\mathcal{R} = 6$ ) since target samples and pre-training samples have different imaging modalities.

Additionally, in Abdomen Atlas and Abdominal MRI datasets, we implemented active few-shot learning to query a few samples to fine-tune the segmentation network on target domains. In Abdomen Atlas, we queried 5% ( $\mathcal{N}_B = 5\%$ ) and 10% ( $\mathcal{N}_B = 10\%$ ) samples, respectively. In the Abdominal MRI dataset, we queried 2 samples ( $\mathcal{N}_B = 2$ ) at each round, and implemented for three rounds in active 3-shot

<sup>1</sup><http://pytorch.org/>

**Table 1**

Performance comparison between our ASFDA, DKD+ASD, and other SOTA methods when adapting Med-VFMs to the AMOS2022-CT domain. The performance was evaluated using Dice scores, and the results were reported as Mean $\pm$ SD. **Bold** and underline represent the best and the second best results (Lower bound 0%: source-training without ADA; Upper bound 100%: fully supervised training).

| Methods  | Low Bound<br>0% | Query Budgets (Number of Iterations) |                                   |                                   |                                  |                                  | Upper Bound<br>100% |
|----------|-----------------|--------------------------------------|-----------------------------------|-----------------------------------|----------------------------------|----------------------------------|---------------------|
|          |                 | 5% (r=1)                             | 10% (r=2)                         | 15% (r=3)                         | 20% (r=4)                        | 25% (r=5)                        |                     |
| RAND     | 0.27 $\pm$ 0.10 | 73.31 $\pm$ 15.50                    | 77.57 $\pm$ 14.65                 | 79.30 $\pm$ 14.40                 | 81.63 $\pm$ 12.87                | 82.30 $\pm$ 12.50                | 93.04 $\pm$ 1.23    |
| ENPY     | 0.27 $\pm$ 0.10 | 74.24 $\pm$ 14.53                    | 78.17 $\pm$ 13.73                 | 80.78 $\pm$ 13.43                 | 82.59 $\pm$ 13.63                | 83.31 $\pm$ 12.05                | 93.04 $\pm$ 1.23    |
| LCON     | 0.27 $\pm$ 0.10 | 73.39 $\pm$ 14.75                    | 77.62 $\pm$ 14.00                 | 80.11 $\pm$ 13.74                 | 82.14 $\pm$ 12.13                | 82.34 $\pm$ 12.36                | 93.04 $\pm$ 1.23    |
| MMAR     | 0.27 $\pm$ 0.10 | 73.92 $\pm$ 14.99                    | 77.63 $\pm$ 13.89                 | 80.44 $\pm$ 13.05                 | 82.23 $\pm$ 13.00                | 82.82 $\pm$ 12.00                | 93.04 $\pm$ 1.23    |
| Core-set | 0.27 $\pm$ 0.10 | 74.42 $\pm$ 14.59                    | 78.55 $\pm$ 13.16                 | 81.11 $\pm$ 12.45                 | 82.73 $\pm$ 12.15                | 84.04 $\pm$ 11.54                | 93.04 $\pm$ 1.23    |
| BADGE    | 0.27 $\pm$ 0.10 | 75.78 $\pm$ 14.28                    | 79.67 $\pm$ 12.94                 | 82.09 $\pm$ 12.50                 | 83.56 $\pm$ 11.95                | 84.69 $\pm$ 10.17                | 93.04 $\pm$ 1.23    |
| SANN     | 0.27 $\pm$ 0.10 | 75.48 $\pm$ 14.17                    | 78.99 $\pm$ 12.43                 | 81.88 $\pm$ 11.17                 | 83.11 $\pm$ 10.89                | 84.45 $\pm$ 10.43                | 93.04 $\pm$ 1.23    |
| UGTST    | 0.27 $\pm$ 0.10 | 75.80 $\pm$ 14.06                    | 80.59 $\pm$ 12.92                 | 82.22 $\pm$ 11.72                 | 83.93 $\pm$ 10.79                | 85.27 $\pm$ 10.72                | 93.04 $\pm$ 1.23    |
| CUP      | 0.27 $\pm$ 0.10 | 73.92 $\pm$ 14.85                    | 77.88 $\pm$ 13.49                 | 80.69 $\pm$ 13.05                 | 82.25 $\pm$ 12.59                | 83.10 $\pm$ 11.70                | 93.04 $\pm$ 1.23    |
| DKD+ASD  | 0.27 $\pm$ 0.10 | <b>78.87<math>\pm</math>13.92</b>    | <u>82.61<math>\pm</math>12.51</u> | <u>84.03<math>\pm</math>10.48</u> | <u>85.54<math>\pm</math>9.74</u> | <u>86.78<math>\pm</math>9.57</u> | 93.04 $\pm$ 1.23    |
| ASFDA    | 0.27 $\pm$ 0.10 | <b>80.51<math>\pm</math>12.53</b>    | <b>84.42<math>\pm</math>11.65</b> | <b>85.52<math>\pm</math>10.06</b> | <b>86.63<math>\pm</math>9.28</b> | <b>87.68<math>\pm</math>9.08</b> | 93.04 $\pm$ 1.23    |

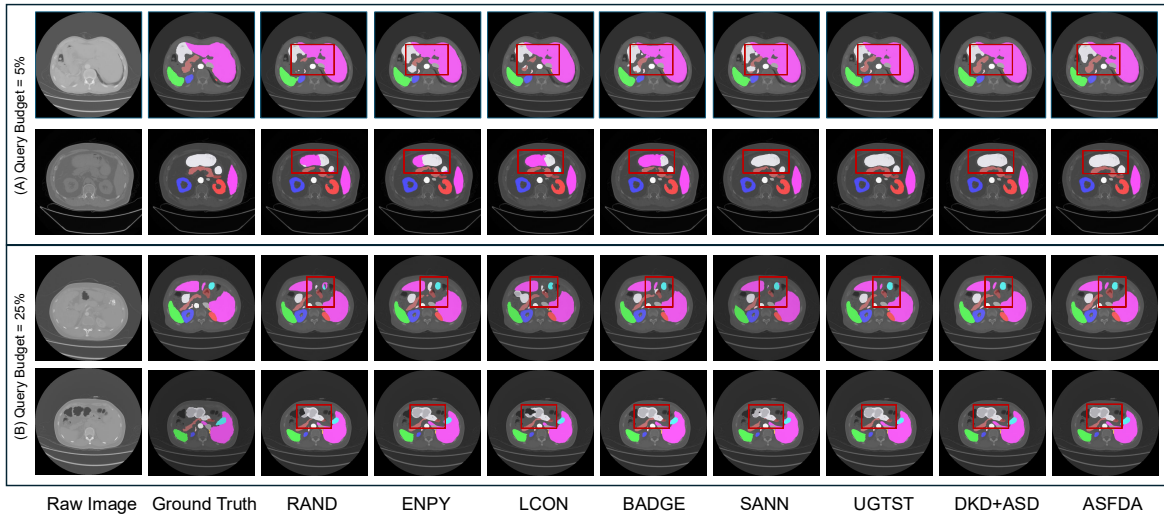


**Figure 2:** Qualitative comparison among results of the Medical Vision Foundation Models fine-tuned by (A) 5% and (B) 25% samples from the AMOS2022-CT domain queried by our methods and other SOTA methods. Red boxes mark the regions where our methods demonstrate better segmentation results than SOTA methods.

learning, active 5-shot learning and active 7-shot learning, respectively.

#### 4.4. Comparison with State-of-the-arts

To fully evaluate the effectiveness of our method, we implemented them in two different ways. First, we implemented the **ASFDA** to adapt the network as Algorithm 1, including Active Test Time Sample Query and Selective Semi-supervised fine-tuning. Additionally, we implemented Active Test Time Sample Query (**DKD+ASD**) by querying samples via DKD and ASD to fine-tune the network in a fully supervised learning without Selective Semi-supervised fine-tuning.

Subsequently, we compared our methods with other commonly used Active Learning strategies, including (1) Random Selection (**RAND**): selecting samples randomly,

(2) Entropy (**ENPY**): an uncertainty-based strategy to select samples with highest entropy in predictive probabilities (Wang and Shang, 2014) (3) Least Confidence (**LCON**): an uncertainty-based strategy to select samples with smallest confidence in prediction probability (Li and Sethi, 2006) (4) Minimal Margin (**MMAR**): an uncertainty-based strategy to select samples with smallest margin in predictive probabilities (Wang and Shang, 2014) (5) A Core set approach (**Core-set**): a diversity-based strategy to select samples by a set-cover problem (Sener and Savarese, 2018) (6) Batch Active learning by Diverse Gradient Embeddings (**BADGE**): a hybrid uncertainty- and diversity-based strategy to select samples from constructing diverse batches by running K-Means++ (Ash et al., 2020). Subsequently, we compared our methods with an Active Learning method which was

**Table 2**

Performance comparison between our ASFDA, DKD+ASD, and other SOTA methods when adapting Med-VFMs to the AMOS2022-MRI domain. The performance was evaluated using Dice scores, and the results were reported as Mean $\pm$ SD. **Bold** and underline represent the best and the second best results (Lower bound 0%: source-training without ADA; Upper bound 100%: fully supervised training).

| Methods  | Low Bound<br>0% | Query Budgets (Number of Iterations) |                          |                          |                          |                         |                         | Upper Bound<br>100% |
|----------|-----------------|--------------------------------------|--------------------------|--------------------------|--------------------------|-------------------------|-------------------------|---------------------|
|          |                 | 5% (r=1)                             | 10% (r=2)                | 15% (r=3)                | 20% (r=4)                | 25% (r=5)               | 30% (r=6)               |                     |
| RAND     | 0.46 $\pm$ 0.13 | 35.84 $\pm$ 27.14                    | 48.06 $\pm$ 25.24        | 55.28 $\pm$ 21.02        | 69.15 $\pm$ 14.46        | 75.56 $\pm$ 12.70       | 77.98 $\pm$ 11.88       | 91.32 $\pm$ 3.74    |
| ENPY     | 0.46 $\pm$ 0.13 | 40.43 $\pm$ 23.29                    | 58.74 $\pm$ 19.88        | 71.16 $\pm$ 14.35        | 76.65 $\pm$ 14.07        | 78.09 $\pm$ 11.85       | 80.94 $\pm$ 9.70        | 91.32 $\pm$ 3.74    |
| LCON     | 0.46 $\pm$ 0.13 | 38.05 $\pm$ 25.62                    | 52.12 $\pm$ 24.57        | 62.35 $\pm$ 18.62        | 73.78 $\pm$ 13.79        | 76.12 $\pm$ 12.44       | 79.29 $\pm$ 11.72       | 91.32 $\pm$ 3.74    |
| MMAR     | 0.46 $\pm$ 0.13 | 38.95 $\pm$ 25.68                    | 55.37 $\pm$ 23.76        | 63.92 $\pm$ 18.67        | 75.79 $\pm$ 13.93        | 77.20 $\pm$ 12.11       | 80.61 $\pm$ 10.94       | 91.32 $\pm$ 3.74    |
| Core-set | 0.46 $\pm$ 0.13 | 41.88 $\pm$ 21.56                    | 63.04 $\pm$ 22.01        | 72.59 $\pm$ 15.91        | 77.24 $\pm$ 11.02        | 78.89 $\pm$ 10.03       | 82.48 $\pm$ 9.18        | 91.32 $\pm$ 3.74    |
| BADGE    | 0.46 $\pm$ 0.13 | 44.00 $\pm$ 21.99                    | 65.49 $\pm$ 19.78        | 75.65 $\pm$ 13.13        | 79.30 $\pm$ 10.98        | 81.31 $\pm$ 10.89       | 82.80 $\pm$ 8.42        | 91.32 $\pm$ 3.74    |
| SANN     | 0.46 $\pm$ 0.13 | 42.03 $\pm$ 24.73                    | 63.13 $\pm$ 22.63        | 74.34 $\pm$ 13.42        | 78.68 $\pm$ 10.70        | 79.19 $\pm$ 10.74       | 82.79 $\pm$ 9.54        | 91.32 $\pm$ 3.74    |
| UGTST    | 0.46 $\pm$ 0.13 | 45.29 $\pm$ 21.30                    | 66.14 $\pm$ 19.20        | 76.45 $\pm$ 12.32        | 80.86 $\pm$ 10.52        | 81.86 $\pm$ 10.49       | 83.53 $\pm$ 8.38        | 91.32 $\pm$ 3.74    |
| CUP      | 0.46 $\pm$ 0.13 | 41.49 $\pm$ 24.83                    | 59.57 $\pm$ 20.87        | 72.17 $\pm$ 14.89        | 77.14 $\pm$ 12.85        | 78.30 $\pm$ 11.17       | 81.62 $\pm$ 9.12        | 91.32 $\pm$ 3.74    |
| DKD+ASD  | 0.46 $\pm$ 0.13 | <b>49.31</b> $\pm$ 20.59             | <u>69.66</u> $\pm$ 18.31 | <u>79.52</u> $\pm$ 11.08 | <u>83.37</u> $\pm$ 10.17 | <u>84.25</u> $\pm$ 9.91 | <u>85.18</u> $\pm$ 8.28 | 91.32 $\pm$ 3.74    |
| ASFDA    | 0.46 $\pm$ 0.13 | <b>52.06</b> $\pm$ 18.12             | <u>72.06</u> $\pm$ 17.70 | <u>81.59</u> $\pm$ 10.39 | <u>85.74</u> $\pm$ 9.98  | <u>86.13</u> $\pm$ 9.47 | <u>86.90</u> $\pm$ 7.67 | 91.32 $\pm$ 3.74    |

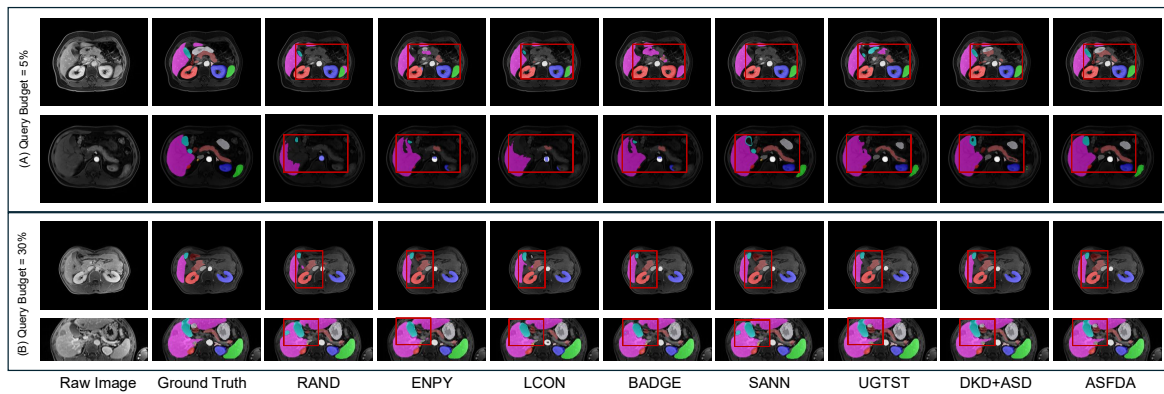


**Figure 3:** Qualitative comparison among results of the Medical Vision Foundation Models fine-tuned by (A) 5% and (B) 30% samples from the AMOS2022-MRI domain queried by our methods and other SOTA methods. Red boxes mark the regions where our methods demonstrate better segmentation results than SOTA methods.

**Table 3**

Performance comparison between our ASFDA, DKD+ASD, and other SOTA methods when adapting Med-VFMs to the FLARE 2021 domain. The performance was evaluated using Dice scores, and the results were reported as Mean $\pm$ SD. **Bold** and underline represent the best and the second best results (Lower bound 0%: source-training without ADA; Upper bound 100%: fully supervised training).

| Methods  | Low Bound<br>0% | Query Budgets (Number of Iterations) |                         |                         |                         |                         | Upper Bound<br>100% |
|----------|-----------------|--------------------------------------|-------------------------|-------------------------|-------------------------|-------------------------|---------------------|
|          |                 | 5% (r=1)                             | 10% (r=2)               | 15% (r=3)               | 20% (r=4)               | 25% (r=5)               |                     |
| RAND     | 5.86 $\pm$ 0.02 | 86.70 $\pm$ 9.93                     | 89.74 $\pm$ 6.23        | 90.57 $\pm$ 5.52        | 91.56 $\pm$ 5.19        | 92.05 $\pm$ 4.18        | 96.85 $\pm$ 1.06    |
| ENPY     | 5.86 $\pm$ 0.02 | 88.71 $\pm$ 7.92                     | 91.54 $\pm$ 4.65        | 92.07 $\pm$ 4.05        | 92.26 $\pm$ 3.91        | 93.35 $\pm$ 3.25        | 96.85 $\pm$ 1.06    |
| LCON     | 5.86 $\pm$ 0.02 | 89.70 $\pm$ 6.49                     | 92.05 $\pm$ 5.11        | 92.91 $\pm$ 3.35        | 93.74 $\pm$ 2.96        | 93.83 $\pm$ 2.62        | 96.85 $\pm$ 1.06    |
| MMAR     | 5.86 $\pm$ 0.02 | 89.68 $\pm$ 5.39                     | 92.08 $\pm$ 4.21        | 92.71 $\pm$ 3.18        | 93.50 $\pm$ 2.66        | 93.84 $\pm$ 2.58        | 96.85 $\pm$ 1.06    |
| Core-set | 5.86 $\pm$ 0.02 | 89.16 $\pm$ 6.46                     | 91.69 $\pm$ 4.23        | 92.61 $\pm$ 3.75        | 92.85 $\pm$ 3.05        | 93.36 $\pm$ 3.19        | 96.85 $\pm$ 1.06    |
| BADGE    | 5.86 $\pm$ 0.02 | 89.51 $\pm$ 5.69                     | 91.77 $\pm$ 4.13        | 92.65 $\pm$ 3.85        | 92.99 $\pm$ 3.53        | 93.80 $\pm$ 2.76        | 96.85 $\pm$ 1.06    |
| SANN     | 5.86 $\pm$ 0.02 | 89.60 $\pm$ 5.44                     | 92.30 $\pm$ 3.80        | 93.43 $\pm$ 3.15        | 93.75 $\pm$ 2.92        | 93.98 $\pm$ 2.91        | 96.85 $\pm$ 1.06    |
| UGTST    | 5.86 $\pm$ 0.02 | 89.56 $\pm$ 5.88                     | 92.15 $\pm$ 3.87        | 93.26 $\pm$ 3.17        | 93.60 $\pm$ 2.67        | 93.70 $\pm$ 3.05        | 96.85 $\pm$ 1.06    |
| CUP      | 5.86 $\pm$ 0.02 | 88.29 $\pm$ 8.87                     | 90.47 $\pm$ 5.39        | 91.59 $\pm$ 4.38        | 91.90 $\pm$ 4.20        | 92.31 $\pm$ 4.12        | 96.85 $\pm$ 1.06    |
| DKD+ASD  | 5.86 $\pm$ 0.02 | <b>91.65</b> $\pm$ 5.09              | <u>93.30</u> $\pm$ 3.68 | <u>93.94</u> $\pm$ 3.08 | <u>94.46</u> $\pm$ 2.78 | <u>94.60</u> $\pm$ 2.53 | 96.85 $\pm$ 1.06    |
| ASFDA    | 5.86 $\pm$ 0.02 | <b>92.52</b> $\pm$ 4.31              | <u>94.08</u> $\pm$ 3.27 | <u>94.33</u> $\pm$ 3.04 | <u>94.54</u> $\pm$ 2.64 | <u>94.87</u> $\pm$ 2.47 | 96.85 $\pm$ 1.06    |

initially proposed for medical image segmentation, termed Suggestive Annotations (**SANN**) (Yang et al., 2017). It is a hybrid uncertainty- and diversity-based strategy to select samples with highest uncertainty in predictive probabilities and lowest semantic similarity. Finally, we compared our methods with other Active Source-free Domain Adaptation methods which were proposed for medical image segmentation, including (1) the Uncertainty-guided Tiered Self-training (**UGTST**): a hybrid uncertainty- and diversity-based strategy to select samples with large aleatoric uncertainty and low neighboring similarity in 2D prostate segmentation from MR images (Luo et al., 2024) and (2) Cascade Uncertainty Predominance (**CUP**): a hybrid uncertainty- and diversity-based strategy to select patches with low uncertainty and large foreground region in UWF-SLO Vessel Segmentation (Wang et al., 2024b).

#### 4.4.1. Experimental results on AMOS2022-CT

We employed our ASFDA method to adapt the Med-VFMs to the AMOS2022-CT domain for volumetric multi-organ segmentation. The fine-tuned network achieved superior performance compared to adaptations using other methods (Table 1). Specifically, querying 5%-25% of the samples with ASFDA yielded 5-8 points higher Dice score than random sample selection. With only 5% queried samples, ASFDA adapted the network to achieve 80.51 Dice score, improving from 0.27 lower bound performance. Moreover, adapting with 25% queried samples by ASFDA fine-tuned the network to reach over 94% of the upper-bound performance in this domain. These results highlight the effectiveness of ASFDA in adapting Med-VFMs to target segmentation domains through efficient sample selection and selective semi-supervised fine-tuning.

We further evaluated the Active Test Time Sample Query strategy (DKD+ASD), and it consistently outperformed other Active Learning query strategies (Table 1). Specifically, UGTST and SANN leveraged hybrid strategies by evaluating uncertainty and diversity, but our strategy adapted the network to achieve 3-4 point higher Dice score with 5% and 10% queried samples, and 1.5-3 points higher with 25% queried samples. Additionally, compared with diversity-based BADGE and uncertainty-based ENPY, our approach achieved the superior adaptation performance of the network by 3-5 points higher Dice score with 5% samples queried.

#### 4.4.2. Experimental results on AMOS2022-MRI

Applying our ASFDA method to adapt the network to the AMOS2022-MRI domain yielded superior performance compared to other adaptation methods (Table 2). With 5% samples queried by our ASFDA method, the network achieved an improvement in adaptation performance of more than 51 points in Dice scores over the lower-bound performance. Additionally, fine-tuning with 30% of the queried samples by our ASFDA enabled the network to reach over 95% of the upper-bound performance in this domain. Moreover, ASFDA improved the adaptation performance of the

network by approximately 16 points higher Dice score compared to adaptation with 5% randomly queried samples, and by 9 points higher Dice score compared to adaptation with 30% randomly selected samples.

We further evaluated the effectiveness of the Active Test Time Sample Query strategy (DKD+ASD) on the AMOS2022-MRI domain. When querying 5% and 30% of the samples for supervised fine-tuning, our strategy enabled the network to achieve improvements in adaptation performance of more than 13 points and 7 points in Dice score compared to adaptation with 5% and 30% randomly queried samples, respectively. Additionally, querying 5% samples by our strategy for fine-tuning enabled the network to achieve more than 5 points higher Dice score than diversity-based BADGE strategy. Similarly, while UGTST queried 5% samples to fine-tune the network by evaluating their uncertainty and diversity, but adapted by our strategy demonstrated 4 points higher Dice score. These results demonstrate the effectiveness of the Active Test Time Sample Query strategy (DKD+ASD) in querying informative samples for adaptation of Med-VFMs.

#### 4.4.3. Experimental results on FLARE 2021

Adapting the Med-VFMs to the FLARE 2021 domain with our ASFDA method resulted in superior performance than other AL or ADA methods (Table 3). With 5% of the samples queried, our method improved the adaptation performance of the network by 87 points from 5.86 points in lower-bound performance to 92.52 points in Dice score. Additionally, fine-tuning the network with 25% queried samples by our ASFDA method enabled it to achieve 97.96% of the upper-bound performance in this domain. Compared to random selection (RAND), adaptation by our method yielded a more significant improvement, demonstrating approximately 5.8 points higher Dice score with 5% queried samples. Additionally, while LCON and MMAR adapted the network by querying 5%-25% of the samples based on predictive confidence, ASFDA consistently achieved 1-3 points higher Dice score.

We also evaluated the Active Test-Time Sample Query strategy (DKD+ASD) on the FLARE2021 domain. Fine-tuning the network with 5%-25% of the samples queried by our strategy achieved 1-2 points higher Dice score than two hybrid uncertainty and diversity-based strategies, including SANN and UGTST. Additionally, with 5% queried samples, our strategy improved the network performance by more than 85 points over the lower-bound performance. Fine-tuning the network with 25% samples queried by our strategy enabled the network to achieve 97.68% of the upper bound performance. These results highlight the effectiveness of our Active Test-Time Sample Query strategy in improving adaptation performance and efficiency.

#### 4.4.4. Experimental results on Abdomen Atlas

Med-VFMs fine-tuned with our ASFDA method achieved superior performance compared to other AL and ADA

methods on the Abdomen Atlas domain (Table 4). Specifically, the network adapted by our ASFDA achieved 83.12 and 84.86 points in Dice scores with 5% and 10% queried samples, respectively, demonstrating approximately 9.4 and 8.1 points higher over random querying (RAND). While SANN, as a hybrid uncertainty- and diversity-based query strategy, optimized the network to achieve higher Dice score than other AL and ADA methods, our ASFDA method adapted the network to demonstrate about 3.6 and 3.3 points higher Dice score than SANN with 5% and 10% queried samples, respectively.

When fine-tuned with samples queried by our Active Test-Time Sample Query strategy (DKD+ASD), the network outperformed those adapted with other query methods (Table 4). Specifically, employing our strategy to query samples for fine-tuning improved the model performance by 8.2 and 7.1 Dice points with 5% and 10% queried samples compared to random selection. Additionally, the network achieved around 2.4 and 2.2 points improvement in Dice score when employing our strategy to query 5% and 10% samples for fine-tuning compared with SANN.

#### 4.4.5. Experimental results on Abdominal MRI

When adapting Med-VFMs to the Abdominal MRI domain, our ASFDA method achieved superior performance compared to other AL and ADA methods (Table 5). The employment of our ASFDA method for active 3-shot learning improved the performance of the source-trained network significantly from approximately 2 to 83.98 Dice points. Additionally, adapted with seven samples queried by our method in active 7-shot learning, the network achieved 88.36 Dice points, demonstrating over 95% of the upper-bound performance (92.95 Dice score). Moreover, the network adapted by our ASFDA method outperformed random querying (RAND) by 17.9, 17.9, and 11.8 points in three respective adaptation rounds. UGTST was designed to evaluate uncertainty and diversity sequentially, and achieved better performance than other AL and ADA methods. However, our ASFDA method consistently outperformed UGTST by approximately 3-6 Dice points throughout the adaptation process.

The network adapted using samples queried by our Active Test-Time Sample Query strategy (DKD+ASD) also demonstrated superior performance over those optimized with alternative AL and ADA methods in the Abdominal MRI domain (Table 5). Specifically, the network adapted by our query strategy achieved better performance compared to UGTST- and SANN-adapted networks by approximately 2.5-4 Dice points in the active few-shot learning setting. Additionally, incorporating DKD and ASD metrics to query sample for fine-tuning, the network achieved approximately 15.3, 15.6, and 11.5 higher points in Dice score compared to random querying in active 3-shot, 5-shot, and 7-shot learning, respectively. These results highlight the effectiveness of our ASFDA method and our Active Test-Time Sample Query strategy in improving few-shot adaptation performance compared to other state-of-the-art strategies.

**Table 4**

Performance comparison between our ASFDA, DKD+ASD, and other SOTA methods when adapting Med-VFMs to the Abdominal Atlas domain. The performance was evaluated using Dice scores, and the results were reported as Mean $\pm$ SD. **Bold** and underline represent the best and the second best results.

| Methods  | Query Budgets           |                         |
|----------|-------------------------|-------------------------|
|          | 5%                      | 10%                     |
| RAND     | 73.74 $\pm$ 11.98       | 76.72 $\pm$ 11.48       |
| ENPY     | 77.39 $\pm$ 10.34       | 80.46 $\pm$ 9.54        |
| LCON     | 74.07 $\pm$ 10.66       | 77.88 $\pm$ 10.90       |
| MMAR     | 75.74 $\pm$ 11.17       | 78.33 $\pm$ 9.81        |
| Core-set | 79.11 $\pm$ 10.20       | 81.44 $\pm$ 9.61        |
| BADGE    | 79.23 $\pm$ 10.01       | 81.48 $\pm$ 9.52        |
| SANN     | 79.56 $\pm$ 9.42        | 81.57 $\pm$ 9.16        |
| UGTST    | 79.43 $\pm$ 10.15       | 81.56 $\pm$ 9.75        |
| CUP      | 77.36 $\pm$ 10.46       | 79.35 $\pm$ 9.92        |
| DKD+ASD  | 81.92 $\pm$ 9.31        | 83.80 $\pm$ 8.70        |
| ASFDA    | <u>83.12</u> $\pm$ 8.16 | <u>84.86</u> $\pm$ 7.52 |

**Table 5**

Performance comparison between our ASFDA, DKD+ASD, and other SOTA methods when adapting Med-VFMs to the Abdominal MRI domain. The performance was evaluated using Dice scores, and the results were reported as Mean $\pm$ SD. **Bold** and underline represent the best and the second best results (Lower bound 0%: source-training without ADA; Upper bound 100%: fully supervised training).

| Methods  | Low Bound<br>0% | Query Budgets (Number of Iterations) |                         |                         | Upper Bound<br>100% |
|----------|-----------------|--------------------------------------|-------------------------|-------------------------|---------------------|
|          |                 | 3-shot (r=1)                         | 5-shot (r=2)            | 7-shot (r=3)            |                     |
| RAND     | 2.01 $\pm$ 0.39 | 66.11 $\pm$ 15.50                    | 69.77 $\pm$ 12.71       | 76.47 $\pm$ 11.32       | 92.95 $\pm$ 1.14    |
| ENPY     | 2.01 $\pm$ 0.39 | 74.10 $\pm$ 12.77                    | 79.52 $\pm$ 11.78       | 81.05 $\pm$ 10.12       | 92.95 $\pm$ 1.14    |
| LCON     | 2.01 $\pm$ 0.39 | 75.46 $\pm$ 12.19                    | 80.32 $\pm$ 11.82       | 82.54 $\pm$ 9.94        | 92.95 $\pm$ 1.14    |
| MMAR     | 2.01 $\pm$ 0.39 | 76.70 $\pm$ 12.25                    | 80.45 $\pm$ 11.20       | 82.76 $\pm$ 9.93        | 92.95 $\pm$ 1.14    |
| Core-set | 2.01 $\pm$ 0.39 | 77.94 $\pm$ 11.15                    | 81.62 $\pm$ 10.82       | 84.21 $\pm$ 9.45        | 92.95 $\pm$ 1.14    |
| BADGE    | 2.01 $\pm$ 0.39 | 77.19 $\pm$ 11.11                    | 81.70 $\pm$ 9.47        | 84.35 $\pm$ 9.39        | 92.95 $\pm$ 1.14    |
| SANN     | 2.01 $\pm$ 0.39 | 77.48 $\pm$ 10.14                    | 82.13 $\pm$ 8.86        | 85.34 $\pm$ 8.44        | 92.95 $\pm$ 1.14    |
| UGTST    | 2.01 $\pm$ 0.39 | 78.11 $\pm$ 9.51                     | 82.21 $\pm$ 8.98        | 85.43 $\pm$ 8.30        | 92.95 $\pm$ 1.14    |
| CUP      | 2.01 $\pm$ 0.39 | 74.92 $\pm$ 12.84                    | 80.22 $\pm$ 11.92       | 81.95 $\pm$ 10.61       | 92.95 $\pm$ 1.14    |
| DKD+ASD  | 2.01 $\pm$ 0.39 | 81.40 $\pm$ 9.41                     | 85.34 $\pm$ 8.91        | 87.95 $\pm$ 8.16        | 92.95 $\pm$ 1.14    |
| ASFDA    | 2.01 $\pm$ 0.39 | <u>83.98</u> $\pm$ 8.29              | <u>87.63</u> $\pm$ 7.47 | <u>88.36</u> $\pm$ 7.32 | 92.95 $\pm$ 1.14    |

#### 4.5. Ablation study

To evaluate the effectiveness of two query metrics, including DKD and ASD, we implemented two ablation studies by employing these two metrics to query 5% and 10% samples for adapting the network to AMOS2022-CT and AMOS2022-MRI domains, separately.

##### 4.5.1. Ablation on the effectiveness of DKD

We implemented the DKD metric to query the top 5% and 10% highest (High DKD) and lowest (Low DKD) scoring samples for adapting the network to AMOS2022-CT and AMOS2022-MRI domains (Table 6). In the AMOS2022-CT domain, adapting the network by 5% and 10% samples with the highest DKD scores achieved 11-12 points higher Dice score compared to adaptation by samples with the lowest scores. Similarly, in the AMOS2022-MRI domain, adaptation of the network by 5% and 10% samples with the

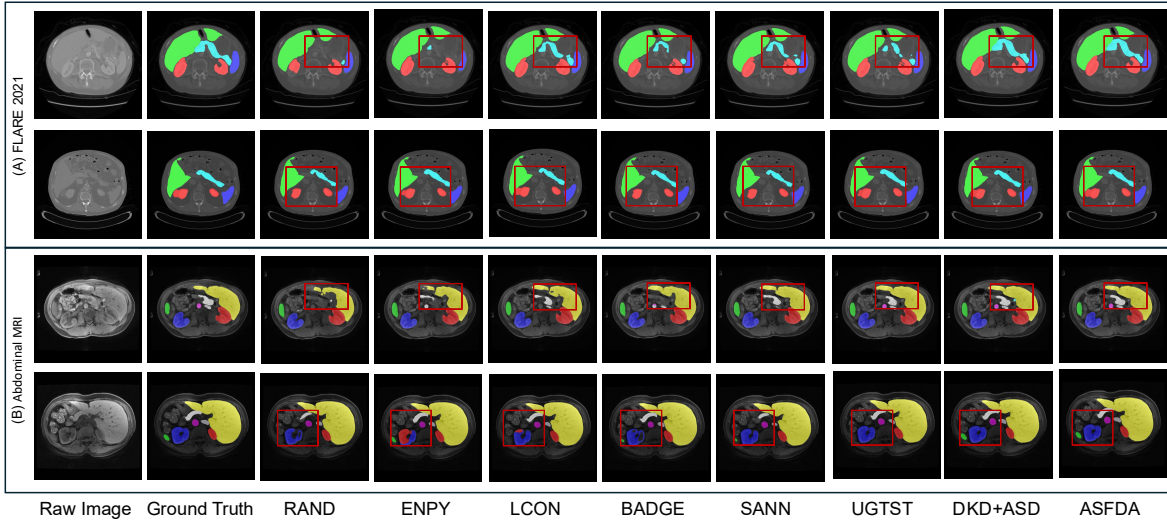


**Figure 4:** Qualitative comparison among results of the Medical Vision Foundation Models fine-tuned by (A) 5% samples from the FLARE2021 domain and (B) 3-shot from the Abdominal MRI domain queried by our methods and other SOTA methods. Red boxes mark the regions where our methods demonstrate better segmentation results than SOTA methods.

**Table 6**

The results of ablation study on DKD metric when adapting Med-VFMs to AMOS2022-CT and AMOS2022-MRI domains. The performance was evaluated using Dice scores, and the results were reported as Mean $\pm$ SD.

| Methods  | AMOS2022-CT       |                   | AMOS2022-MR       |                   |
|----------|-------------------|-------------------|-------------------|-------------------|
|          | 5%                | 10%               | 5%                | 10%               |
| RAND     | 73.31 $\pm$ 15.50 | 77.57 $\pm$ 14.65 | 35.84 $\pm$ 27.14 | 48.06 $\pm$ 25.24 |
| High DKD | 76.14 $\pm$ 13.67 | 79.48 $\pm$ 12.56 | 45.23 $\pm$ 20.89 | 64.46 $\pm$ 19.56 |
| Low DKD  | 64.48 $\pm$ 14.72 | 68.20 $\pm$ 14.83 | 26.86 $\pm$ 22.67 | 42.59 $\pm$ 20.75 |

highest DKD scores demonstrated better performance than the adaptation by the lowest DKD scoring samples, demonstrating 9-11 points higher Dice score. Additionally, fine-tuning the network with high-DKD samples consistently achieved better performance than random selection. These results demonstrate that evaluating the DKD metric effectively identifies informative samples, and querying samples with high DKD scores for fine-tuning the network improves adaptation performance compared to random selection.

#### 4.5.2. Ablation on the effectiveness of ASD

To evaluate the effectiveness of the ASD metric in measuring sample informativeness, we adapted the network to the AMOS2022-CT and AMOS2022-MRI domains by querying the top 5% and 10% samples with the highest ASD scores (High ASD) and the lowest ASD scores (Low ASD) (Table 7). Specifically, in both domains, adapting the network with 5% and 10% high ASD samples consistently outperformed adaptation with low ASD samples. Thus, querying samples with high ASD scores effectively identifies the informative samples, and adapting the network with high ASD scores improves the adaptation performance.

We examined the impact of applying binary masks by comparing adaptation performance of our ASD and ENPY.

**Table 7**

The results of ablation study on ASD metric when adapting Med-VFMs to AMOS2022-CT and AMOS2022-MRI domains. The performance was evaluated using Dice scores, and the results were reported as Mean $\pm$ SD.

| Methods  | Temperature function | AMOS2022-CT       |                   | AMOS2022-MR       |                   |
|----------|----------------------|-------------------|-------------------|-------------------|-------------------|
|          |                      | 5%                | 10%               | 5%                | 10%               |
| ENPY     | -                    | 74.24 $\pm$ 14.53 | 78.17 $\pm$ 13.73 | 40.43 $\pm$ 23.29 | 58.74 $\pm$ 19.88 |
| High ASD | $\tau = 1$           | 75.30 $\pm$ 14.98 | 79.13 $\pm$ 13.69 | 42.39 $\pm$ 21.50 | 61.45 $\pm$ 19.14 |
| Low ASD  | $\tau = 1$           | 62.96 $\pm$ 15.36 | 63.57 $\pm$ 14.35 | 29.05 $\pm$ 22.38 | 39.08 $\pm$ 20.13 |
| High ASD | $\tau(r)$            | 75.92 $\pm$ 14.39 | 79.41 $\pm$ 13.24 | 44.10 $\pm$ 20.41 | 63.77 $\pm$ 18.48 |
| Low ASD  | $\tau(r)$            | 64.73 $\pm$ 15.44 | 66.43 $\pm$ 13.88 | 29.64 $\pm$ 21.35 | 40.15 $\pm$ 19.49 |

ENPY was employed to query samples with high entropy values which were calculated from the whole samples without applying a binary mask. Adapting the network with high ASD samples outperformed ENPY by approximately 1-3 Dice points in both domains when 5% and 10% samples were queried (Table 7). We further evaluated the impact of the dynamic temperature scaling function by evaluating adaptation performance across different temperature values  $\tau$  in the ASD metric (Table 7). In both domains, adapting the network with high ASD samples improved the Dice score by 1-1.5 points when the dynamic temperature scaling function was applied ( $\tau(r)$ ), compared with ASD querying without temperature scaling ( $\tau = 1$ ). These results demonstrate the effectiveness of incorporating the dynamic temperature scaling function into the ASD metric, thus highlighting the importance of the dynamic temperature scaling function in Eq. 7.

#### 4.5.3. Ablation on Selective Semi-supervised Fine-tuning

The employment of Selective Semi-supervised Fine-tuning enhanced the adaptation performance of Med-VFMs

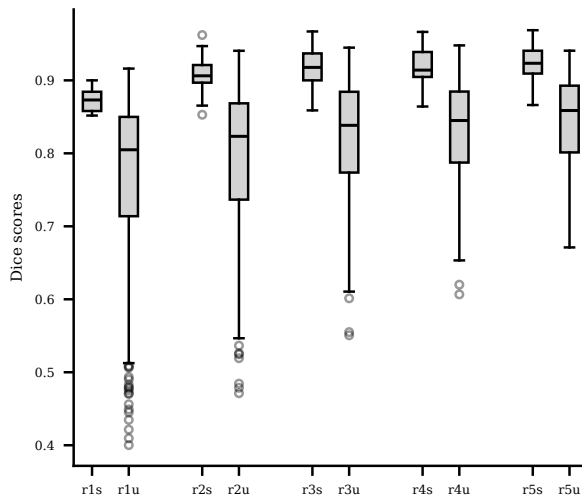


**Figure 5:** Comparison of distributions of Dice scores from selected (s) unlabeled samples for the Selective Semi-supervised Fine-tuning and unselected (u) unlabeled samples when adapting Med-VFMs to the AMOS2022-CT domain for five rounds (r1, r2, r3, r4, and r5).

across multiple segmentation domains. For the AMOS2022-CT domain, incorporating this strategy with Active Test Time Sample Query strategy in our ASFDA method improved the performance by approximately 1-2 Dice points (Table 1). When adapting to the AMOS2022-MRI domain with 5%-30% samples queried by our Active Test Time Sample Query strategy (DKD+ASD), Selective Semi-supervised Fine-tuning further improved the performance by 2-3 Dice points (Table 2). Similarly, in the FLARE 2021 domain, employing Selective Semi-supervised Fine-tuning in our ASFDA method improved the segmentation performance of Med-VFMs by approximately 0.5-1 Dice points compared to the sole use of the query strategy (Table 3). Finally, in Abdomen Atlas and Abdominal MRI domains, applying Selective Semi-supervised Fine-tuning within our ASFDA method improved segmentation performance by approximately 1.2 and 2.5 Dice points, respectively (Table 4 and 5). These results highlight that Selective Semi-Supervised Fine-Tuning provides consistent benefits in adaptation performance of Med-VFMs to our ASFDA methods across diverse domains.

#### 4.6. Analysis on the effectiveness of Selective Semi-supervised Fine-tuning

The goal of the selection mechanism in Selective Semi-supervised Fine-tuning is to select reliable unlabeled samples  $\mathbf{X}_{t,u}^r$  for generating high-quality pseudo labels  $\mathbf{Y}_{t,u}^r$  from unlabeled target sets  $\mathbb{T}_u$ . To demonstrate the effectiveness of this selection mechanism, we compared the distributions in Dice scores of selected unlabeled samples and unselected unlabeled samples. We adapted the Med-VFMs to the AMOS2022-CT domain for five rounds ( $r=1, 2, 3, 4, 5$ ), and

**Table 8**

The p-values of Mann-whitney u test on differences in Dice scores between selected samples and unselected samples in Selective Semi-supervised Fine-tuning when adapting Med-VFMs to the AMOS2022-CT domain.

| Query budgets | 5% (r1)               | 10% (r2)               | 15% (r3)               | 20% (r4)               | 25% (r5)               |
|---------------|-----------------------|------------------------|------------------------|------------------------|------------------------|
| p-values      | $3.97 \times 10^{-6}$ | $4.53 \times 10^{-13}$ | $5.12 \times 10^{-17}$ | $5.06 \times 10^{-20}$ | $1.80 \times 10^{-22}$ |

showed dice scores for selected and unselected samples at each round (r1s, r2s, r3s, r4s, r5s, and, r1u, r2u, r3u, r4u, r5u) (Figure 5). The Dice scores of selected unlabeled samples were obviously higher than unselected unlabeled samples at each round.

Second, we implemented Mann-Whitney U test to demonstrate whether the differences in distributions of these two groups were significant (Table 8). The p-values of Mann-whitney U test were much smaller than 0.01 at each round, demonstrating that the differences of Dice scores between selected and unselected samples were significant. Thus, employing our selection mechanism in Selective Semi-supervised Fine-tuning enables the models to select reliable samples from unlabeled sets for generating high-quality pseudo labels.

## 5. Conclusion

We propose the first Active Source-Free Domain Adaptation method to efficiently adapt Medical Vision Foundation Models to target domains for volumetric medical image segmentation. This ASFDA method introduces a novel Active Learning strategy to select the most informative samples from the target domains for fine-tuning Med-VFMs without requiring access to source pre-training samples. It enables high adaptation performance under a minimal sample selection budget. In this AL method, we design an Active Test Time Sample Query strategy to select samples from the target domains based on two query metrics, including Diversified Knowledge Divergence and Anatomical Segmentation Difficulty. Additionally, our ASFDA method integrates Selective Semi-supervised Fine-tuning to enhance the performance and efficiency of adaptation. We validate our method by adapting Med-VFMs across five domains for volumetric medical image segmentation. The extensive experimental results demonstrate that our method consistently achieves superior performance compared to state-of-the-art methods.

## Declaration of competing interests

The authors declare that they have no known competing financial interests or personal relationships that could have appeared to influence the work reported in this paper.

## Acknowledgments

This work was supported by the National Institutes of Health grants U24 CA258483. Computations were performed using the facilities of the Washington University

Research Computing and Informatics Facility (RCIF). The RCIF has received funding from NIH S10 program grants: 1S10OD025200-01A1 and 1S10OD030477-01.

## CRediT authorship contribution statement

JY: conceptualization, methodology, formal analysis, writing the original draft, reviewing, and editing, visualization; DM: methodology, writing, reviewing, and editing, supervision; AS: methodology, writing, reviewing, and editing, supervision.

## References

Ash, J.T., Zhang, C., Krishnamurthy, A., Langford, J., Agarwal, A., 2020. Deep batch active learning by diverse, uncertain gradient lower bounds, in: International Conference on Learning Representations.

Du, Z., Li, J., 2023. Diffusion-based probabilistic uncertainty estimation for active domain adaptation. *Advances in Neural Information Processing Systems* 36, 17129–17155.

Gaillochet, M., Desrosiers, C., Lombaert, H., 2023. Active learning for medical image segmentation with stochastic batches. *Medical Image Analysis* 90, 102958.

He, J., Liu, B., Yin, G., 2024. Enhancing semi-supervised domain adaptation via effective target labeling, in: Proceedings of the AAAI Conference on Artificial Intelligence, pp. 12385–12393.

He, K., Zhang, X., Ren, S., Sun, J., 2015. Delving deep into rectifiers: Surpassing human-level performance on imagenet classification, in: Proceedings of the IEEE international conference on computer vision, pp. 1026–1034.

Hiasa, Y., Otake, Y., Takao, M., Ogawa, T., Sugano, N., Sato, Y., 2019. Automated muscle segmentation from clinical ct using bayesian u-net for personalized musculoskeletal modeling. *IEEE transactions on medical imaging* 39, 1030–1040.

Ji, Y., Bai, H., Ge, C., Yang, J., Zhu, Y., Zhang, R., Li, Z., Zhanng, L., Ma, W., Wan, X., et al., 2022. Amos: A large-scale abdominal multi-organ benchmark for versatile medical image segmentation. *Advances in neural information processing systems* 35, 36722–36732.

Kothandaraman, D., Shekhar, S., Sancheti, A., Ghuhan, M., Shukla, T., Manocha, D., 2023. Salad: Source-free active label-agnostic domain adaptation for classification, segmentation and detection, in: Proceedings of the IEEE/CVF Winter Conference on Applications of Computer Vision, pp. 382–391.

Li, M., Sethi, I.K., 2006. Confidence-based active learning. *IEEE transactions on pattern analysis and machine intelligence* 28, 1251–1261.

Li, R., Zhang, B., Liu, J., Liu, W., Zhao, J., Teng, Z., 2023a. Heterogeneous diversity driven active learning for multi-object tracking, in: Proceedings of the IEEE/CVF International Conference on Computer Vision, pp. 9932–9941.

Li, S., Zhang, R., Gong, K., Xie, M., Ma, W., Gao, G., 2023b. Source-free active domain adaptation via augmentation-based sample query and progressive model adaptation. *IEEE Transactions on Neural Networks and Learning Systems* .

Li, W., Yuille, A., Zhou, Z., 2025. How well do supervised 3d models transfer to medical imaging tasks? *arXiv preprint arXiv:2501.11253* .

Li, X., Xia, M., Jiao, J., Zhou, S., Chang, C., Wang, Y., Guo, Y., 2023c. Hal-ia: A hybrid active learning framework using interactive annotation for medical image segmentation. *Medical Image Analysis* 88, 102862.

Luo, Z., Luo, X., Gao, Z., Wang, G., 2024. An uncertainty-guided tiered self-training framework for active source-free domain adaptation in prostate segmentation, in: International Conference on Medical Image Computing and Computer-Assisted Intervention, Springer, pp. 107–117.

Ma, J., Zhang, Y., Gu, S., An, X., Wang, Z., Ge, C., Wang, C., Zhang, F., Wang, Y., Xu, Y., et al., 2022. Fast and low-gpu-memory abdomen ct organ segmentation: the flare challenge. *Medical Image Analysis* 82, 102616.

Mahapatra, D., Tennakoon, R., George, Y., Roy, S., Bozorgtabar, B., Ge, Z., Reyes, M., 2024. Alfredo: Active learning with feature disentanglement and domain adaptation for medical image classification. *Medical image analysis* 97, 103261.

Moor, M., Banerjee, O., Abad, Z.S.H., Krumholz, H.M., Leskovec, J., Topol, E.J., Rajpurkar, P., 2023. Foundation models for generalist medical artificial intelligence. *Nature* 616, 259–265.

Nath, V., Yang, D., Landman, B.A., Xu, D., Roth, H.R., 2020. Diminishing uncertainty within the training pool: Active learning for medical image segmentation. *IEEE Transactions on Medical Imaging* 40, 2534–2547.

Ning, M., Lu, D., Wei, D., Bian, C., Yuan, C., Yu, S., Ma, K., Zheng, Y., 2021. Multi-anchor active domain adaptation for semantic segmentation, in: Proceedings of the IEEE/CVF international conference on computer vision, pp. 9112–9122.

Pai, S., Hadzic, I., Bontempi, D., Bressem, K., Kann, B.H., Fedorov, A., Mak, R.H., Aerts, H.J., 2025. Vision foundation models for computed tomography. *arXiv preprint arXiv:2501.09001* .

Ronneberger, O., Fischer, P., Brox, T., 2015. U-net: Convolutional networks for biomedical image segmentation, in: International Conference on Medical image computing and computer-assisted intervention, Springer, pp. 234–241.

Sener, O., Savarese, S., 2018. Active learning for convolutional neural networks: A core-set approach, in: International Conference on Learning Representations. URL: <https://openreview.net/forum?id=H1aIuk-RW>.

Settles, B., 2011. From theories to queries: Active learning in practice, in: Active learning and experimental design workshop in conjunction with AISTATS 2010, JMLR Workshop and Conference Proceedings, pp. 1–18.

Shu, X., Li, Z., Tian, C., Chang, X., Yuan, D., 2025. An active learning model based on image similarity for skin lesion segmentation. *Neurocomputing* , 129690.

Siddiqui, Y., Valentin, J., Nießner, M., 2020. Viewal: Active learning with viewpoint entropy for semantic segmentation, in: Proceedings of the IEEE/CVF conference on computer vision and pattern recognition, pp. 9433–9443.

Wang, D., Shang, Y., 2014. A new active labeling method for deep learning, in: 2014 International joint conference on neural networks (IJCNN), IEEE, pp. 112–119.

Wang, F., Han, Z., Zhang, Z., He, R., Yin, Y., 2023. Mhpl: Minimum happy points learning for active source free domain adaptation, in: Proceedings of the IEEE/CVF Conference on Computer Vision and Pattern Recognition, pp. 20008–20018.

Wang, H., Chen, J., Zhang, S., He, Y., Xu, J., Wu, M., He, J., Liao, W., Luo, X., 2024a. Dual-reference source-free active domain adaptation for nasopharyngeal carcinoma tumor segmentation across multiple hospitals. *IEEE Transactions on Medical Imaging* .

Wang, H., Luo, X., Chen, W., Tang, Q., Xin, M., Wang, Q., Zhu, L., 2024b. Advancing uwf-slo vessel segmentation with source-free active domain adaptation and a novel multi-center dataset, in: International Conference on Medical Image Computing and Computer-Assisted Intervention, Springer, pp. 75–85.

Wang, S., Safari, M., Li, Q., Chang, C.W., Qiu, R.L., Roper, J., Yu, D.S., Yang, X., 2025. Triad: Vision foundation model for 3d magnetic resonance imaging. *arXiv preprint arXiv:2502.14064* .

Wang, X., Lian, L., Yu, S.X., 2022. Unsupervised selective labeling for more effective semi-supervised learning, in: European conference on computer vision, Springer, pp. 427–445.

Wu, T.H., Liu, Y.C., Huang, Y.K., Lee, H.Y., Su, H.T., Huang, P.C., Hsu, W.H., 2021. Redal: Region-based and diversity-aware active learning for point cloud semantic segmentation, in: Proceedings of the IEEE/CVF international conference on computer vision, pp. 15510–15519.

Xie, B., Yuan, L., Li, S., Liu, C.H., Cheng, X., 2022. Towards fewer annotations: Active learning via region impurity and prediction uncertainty for domain adaptive semantic segmentation, in: Proceedings of the IEEE/CVF conference on computer vision and pattern recognition, pp. 8068–8078.

Yang, C., Huang, L., Crowley, E.J., 2024. Plug and play active learning for object detection, in: Proceedings of the IEEE/CVF conference on

computer vision and pattern recognition, pp. 17784–17793.

Yang, L., Zhang, Y., Chen, J., Zhang, S., Chen, D.Z., 2017. Suggestive annotation: A deep active learning framework for biomedical image segmentation, in: Medical Image Computing and Computer Assisted Intervention- MICCAI 2017: 20th International Conference, Quebec City, QC, Canada, September 11-13, 2017, Proceedings, Part III 20, Springer pp. 399–407.

Zhang, S., Metaxas, D., 2024. On the challenges and perspectives of foundation models for medical image analysis. *Medical image analysis* 91, 102996.

Zhang, W., Lv, Z., Zhou, H., Liu, J.W., Li, J., Li, M., Li, Y., Zhang, D., Zhuang, Y., Tang, S., 2024. Revisiting the domain shift and sample uncertainty in multi-source active domain transfer, in: Proceedings of the IEEE/CVF Conference on Computer Vision and Pattern Recognition, pp. 16751–16761.

Zhao, Z., Zeng, Z., Xu, K., Chen, C., Guan, C., 2021. Dsal: Deeply supervised active learning from strong and weak labelers for biomedical image segmentation. *IEEE journal of biomedical and health informatics* 25, 3744–3751.

Zhou, A., Liu, Z., Tieu, A., Patel, N., Sun, S., Yang, A., Choi, P., Lee, H.C., Tordjman, M., Deyer, L., et al., 2025. Mrannotator: multi-anatomy and many-sequence mri segmentation of 44 structures. *Radiology Advances* 2, umae035.

Zhou, T., Yang, J., Cui, L., Zhang, N., Chai, S., 2024. Sbc-al: Structure and boundary consistency-based active learning for medical image segmentation, in: International Conference on Medical Image Computing and Computer-Assisted Intervention, Springer. pp. 283–293.

Zhou, Y., Chia, M.A., Wagner, S.K., Ayhan, M.S., Williamson, D.J., Struyven, R.R., Liu, T., Xu, M., Lozano, M.G., Woodward-Court, P., et al., 2023. A foundation model for generalizable disease detection from retinal images. *Nature* 622, 156–163.

Zhu, W., Huang, H., Tang, H., Musthyala, R., Yu, B., Chen, L., Vega, E., O'Donnell, T., Dehkharghani, S., Frontera, J.A., et al., 2025. 3d foundation ai model for generalizable disease detection in head computed tomography. *arXiv preprint arXiv:2502.02779* .